

Efficient Additive Gaussian Process Regression for Large-scale Data and Application to Analysis of Hourly-recorded NO₂ Concentrations in London

Sahoko Ishida, Wicher Bergsma

London School of Economics and Political Science

Abstract

This paper focuses on statistical modelling using additive Gaussian process (GP) models and their efficient implementation for large-scale spatio-temporal data with a multi-dimensional grid structure. To achieve this, we exploit the Kronecker product structures of the covariance kernel. While this method has gained popularity in the GP literature, the existing approach is limited to covariance kernels with a tensor product structure and does not allow flexible modelling and selection of interaction effects. This is considered an important component in spatio-temporal analysis. We extend the method to a more general class of additive GP models that accounts for main effects and selected interaction effects. Our approach allows for easy identification and interpretation of interaction effects. The proposed model is applied to the analysis of NO₂ concentrations during the COVID-19 lockdown in London. Our scalable method enables analysis of large-scale, hourly-recorded data collected from 59 different stations across the city, providing additional insights to findings from previous research using daily or weekly averaged data.

1 Introduction

Gaussian process (GP) regression has gained increasing attention in recent years, particularly within the machine learning community. The kernel, or covariance function, of a GP plays a critical role in establishing the relationship between predictors and the response variable, and a variety of kernel options allow for flexibility in modelling complex relationships. Through its use of kernel functions, GPs are well-suited for handling auto-correlated data, making them a natural choice for applications in fields such as epidemiology, environmental science, and climate studies, where accounting for auto-correlation in both spatial and temporal domains is crucial. GP regression has a long history in spatial and spatio-temporal analysis and is closely connected to well-established methods, such as Kriging (Krige, 1951; Matheron, 1963) for geostatistical data, log-Gaussian Cox processes (Møller et al., 1998) for modelling spatial and spatio-temporal point processes (Diggle et al., 2013) and a family of conditional auto-regressive models for areal data (see D. Lee (2011) for an overview).

Environmental monitoring and forecasting has benefited from the application of GP regression in various studies (Datta et al., 2016; Grancharova et al., 2008; Liu et al., 2018; Patel et al., 2022; Petelin et al., 2013). With the COVID-19 pandemic, air quality monitoring has gained renewed attention as the lockdown

measures have led to changes in traffic and industrial activities, the major sources of air-pollutant emissions. Researchers have used data collected from monitoring sites in different regions and various statistical methods to investigate the impact of restricted mobility on air quality. Examples of such studies include Solberg et al. (2021), Fioravanti et al. (2022), J. D. Lee et al. (2020), and Cameletti (2020).

1.1 Hourly-recorded NO₂ concentrations in London

In this paper, we analyze a large dataset of hourly-recorded NO₂ concentrations in London, comprising over 200,000 data points collected from 59 air quality monitoring stations over 147 days between January 6th and May 31st, 2020. As the data exhibits spatial, temporal and periodic patterns, a careful approach is needed to model it effectively. To account for the hourly cyclical pattern and potential interaction effects, we adopt additive Gaussian process (GP) models to analyze the response variable, $y_{s,d,h}$, representing the NO₂ concentration at a monitoring station s , on day d and at hour h . The model is given by

$$y_{s,d,h} = f(\mathbf{x}_{1s}, x_{2d}, x_{3h}) + \epsilon_{s,d,h} \quad (1.1)$$

where $\epsilon_{s,d,h}$ is an error term, and $\mathbf{x}_{1s}, x_{2d}, x_{3h}$ represents the three predictors: two dimensional geo-graphical coordinate of station s , day number d and hour of the day h . The specification for $f(\mathbf{x}_{1s}, x_{2d}, x_{3h})$ carries one's assumptions on the model. One example can be given by

$$f(\mathbf{x}_{1s}, x_{2d}, x_{3h}) = a + f_1(\mathbf{x}_{1s}) + f_2(x_{2d}) + f_3(x_{3h}) + f_{12}(\mathbf{x}_{1s}, x_{2d}) + f_{13}(\mathbf{x}_{1s}, x_{3h}) + f_{23}(x_{2d}, x_{3h}). \quad (1.2)$$

In this model, the first term after the constant a captures spatial patterns, while the second and third terms model the global time trend and daily cyclical effect, respectively. In addition to the main effects, we include two-way interaction effects, represented in $f_{12}(\mathbf{x}_{1s}, x_{2d})$, $f_{13}(\mathbf{x}_{1s}, x_{3h})$ and $f_{23}(x_{2d}, x_{3h})$ to capture how these effects vary across locations and time. For example, the last term $f_{23}(x_{2d}, x_{3h})$ accounts for the interaction effect between global time and hour of the day, reflecting the belief that the daily cycle changes over time. We can explore simpler models with only main terms or a subset of interaction effects. If all two-way interactions are present, we can consider a saturated model with the three-way interaction effect $f_{123}(\mathbf{x}_{1s}, x_{2d}, x_{3h})$, which gives a saturated model. The models considered for this dataset are listed in Section 4.2. The main idea of additive GP models is that we assume each function in to follow a GP. Additive GP models have not been extensively explored for analyzing hourly-recorded air quality measurements of this size, except for a few examples such as Pinder et al. (2021).

1.2 Methodological challenges and our contributions

Researchers often encounter obstacles when using GP regression to analyse complex data structures. As aforementioned, important component of modeling with Gaussian process is its kernel. While kernel learning for a complex data structure has been a popular topic in machine learning communities, the aspect of statistical modelling has received much less attention. To be useful for modelling real-world data, GP models must be able to handle main and interaction effects in an intuitive and interpretable way. However, using GP in practice poses computational challenges due to time complexity $O(n^3)$ and storage requirement $O(n^2)$. The data used for air quality monitoring purpose are collected from different measurement stations, for a long period of time. This easily leads to thousands and millions of data points, which is deemed prohibitive in standard GP regression. As a result, environmental monitoring studies often scale down the

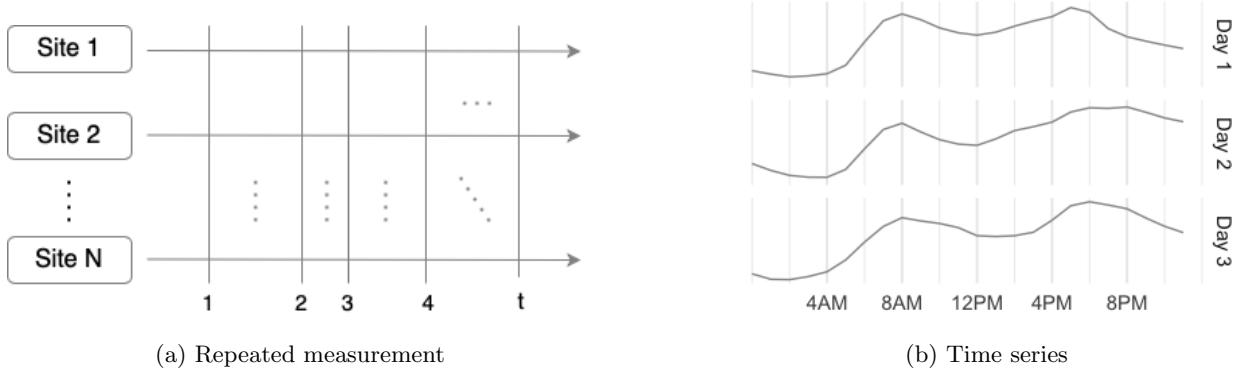


Figure 1: Example of data with multidimensional grid structure. The left panel is an example of repeated measurements from different sites. This can also be seen as a series of time series. The right panel illustrates that each time series with periodicity (e.g. daily cycle) also has a two dimensional grid structure.

data by limiting the number of measurement sites or modeling daily or weekly averaged data. We address these issues by the following.

1. Hierarchical ANOVA kernel for statistical modelling with additive GP

Additive Gaussian process models (Duvenaud et al., 2011; Plate, 1999) are a class of models that assume the regression function has an additive form similar to Generalized Additive Models (GAMs, Hastie and Tibshirani (1990)). In this class of models, each function follows a GP. The main idea of Duvenaud et al. (2011) is to construct each interaction term as a tensor product of the main effect functions. This can be achieved by multiplying the kernel of the main effect functions, which is called the tensor product kernel. This approach is closely related to the ANOVA decomposition kernel (Durrande et al., 2013; Stitson et al., 1999), which consists of main terms and all interaction terms up to the highest orders, corresponding to a saturated model that considers all possible interaction effects. In this paper, we use a hierarchical ANOVA decomposition kernel that does not necessarily assume all possible interaction effects. As with any statistical modelling problem, interaction terms are included along with main terms and any lower-order interaction terms. We also demonstrate that the resulting fitted regression model is easily interpretable.

2. Kronecker approach for large-scale data

There are various approaches to reduce the computational burden of GP models (see Liu et al. (2020) for an overview), many with many relying on approximations to the covariance matrix. For instance, Datta et al. (2016) introduced dynamic nearest neighbour GP that induces a sparse structure in the inverse of the covariance matrix with non-separable kernel structures. They successfully applied this method to analyze air pollution data similar in size to the data in our study. In contrast, our approach for efficient implementation of the proposed model does not resort to approximations. Instead, we leverage the common data structure present in spatio-temporal data, producing exact results, producing the exact result. Specifically, we use Kronecker methods, which are applicable to multidimensional grid structures, which can also be understood as multi-level panel data commonly found in environmental monitoring. For example, measurements from different environmental monitoring stations are often recorded at the same timestamps, giving two-dimensional grid data. It is also worth noting that timestamps do not necessarily have to be in a regular interval. Interestingly, single time series data with periodicity, such as the daily cycle commonly observed in ambient air pollutant concentrations, can also be treated as two-dimensional grid data. Figure 1 illustrates these examples. The previous work by Flaxman et al. (2015), Gilboa et al. (2013), Saatçi (2012), and Wilson et al. (2014) has

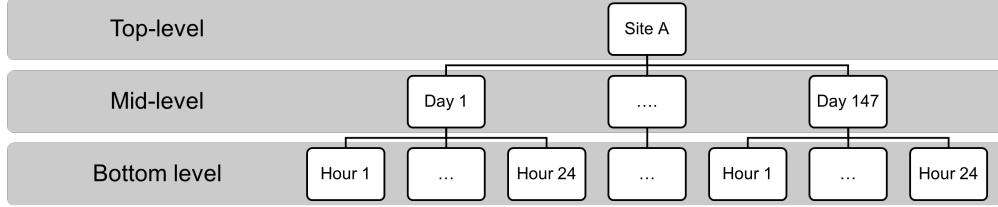


Figure 2: The structure of the NO₂ dataset

shown that the covariance matrix for this type of data can be expressed as Kronecker products. By exploiting the properties of Kronecker products, computational complexity and storage requirements can be reduced to $O(n)$ in the best case. However, these methods were only applicable to limited submodels, such as the saturated models or models with only the highest ordered interaction terms. This implies that general additive models, such as main effect or non-saturated interaction effect models, still face constraints with $O(n^3)$ computations and $O(n^2)$ storage. In this paper, we show that Kronecker methods can be made more flexible to handle more general cases, thanks to the centring of kernels. This allows us to model larger-scale data with many structures, including, but not limited to, saturated models.

We applied the proposed method to analyze the previously mentioned NO₂ concentration data. The structure of the dataset can be viewed as a combination of the two examples shown in Figure 1a and 1b, resulting in a three-dimensional grid structure (as depicted in Figure 2) with monitoring station, calendar date, and hour of the day as the top-level, middle-level, and bottom-level, respectively. This allowed us to efficiently implement the models with various structures. The model comparison suggests that the best fit for the data is a non-saturated interaction model, which would have been difficult to fit for a dataset of this size. Our data analysis, which used hourly-recorded data collected from 59 stations over 21 weeks, identified spatial, temporal, and periodic patterns in the data and how they interact with each other. These patterns and effects can easily be visualised and interpreted.

1.3 Organization of the work

The rest of the paper is structured as follows. In Section 2, we present the proposed additive GP models with a hierarchical ANOVA kernel. centring of kernels is also introduced in this section. Section 3 describes our approach to efficient implementation of the proposed model for multi-dimensional grid structured data, by exploiting the Kronecker product structure in the model covariance matrix. The models and methods in Section 2 and 3 are described with two-dimensional grid data or two predictors models as the main motivating example. The reason for this is that the key concepts and advantages can be effectively illustrated with this simple setting. Each section then will include a generalisation to the higher-dimensional case so that the proposed models and methods can be incorporated to other applications such as time-series analysis, repeated measurements in psychology and medical science, and image analysis. The details of our application are discussed in Section 4, including data description, model formulation, results and their interpretation.

2 Additive Gaussian process model

Let \mathcal{X}_1 and \mathcal{X}_2 be nonempty sets. Consider a regression model for two predictors $\mathbf{x}_1 \in \mathcal{X}_1, \mathbf{x}_2 \in \mathcal{X}_2$, and a real-valued response y . In the example in Figure 1a, \mathbf{x}_1 can be the location of the sites expressed in a set of coordinates and \mathbf{x}_2 is a timestamp numbered from 0, 1, If the data is expressed in a long format and n is the total number of observations, for $i = 1, \dots, n$, the model is expressed as

$$y_i = f(\mathbf{x}_{1i}, \mathbf{x}_{2i}) + \epsilon_i \quad (2.1)$$

where the error terms $(\epsilon_1, \dots, \epsilon_n) \sim \mathbf{MVN}(\mathbf{0}, \Sigma)$. For i.i.d errors, we write $\Sigma = \sigma^2 \mathbf{I}_n$ where \mathbf{I}_n is the $n \times n$ identity matrix. Given two predictors and a constant a , it is natural to consider following additive models:

$$f(\mathbf{x}_{1i}, \mathbf{x}_{2i}) = a + f_1(\mathbf{x}_{1i}) + f_2(\mathbf{x}_{2i}) \quad (2.2)$$

$$f(\mathbf{x}_{1i}, \mathbf{x}_{2i}) = a + f_1(\mathbf{x}_{1i}) + f_2(\mathbf{x}_{2i}) + f_{12}(\mathbf{x}_{1i}, \mathbf{x}_{2i}). \quad (2.3)$$

While the first represents the main effect model, the second assumes an additional interaction effect between the two predictors. The main idea of additive GP models is to put a GP prior on each function f_1, f_2 and f_{12} in (2.2) and (2.3). The model formulation above is not restricted to the two-dimensional grid structure and it is applicable to any regression problems with two predictors. We will re-formulate the same models in Section 3 for two-dimensional grid structure data and show how the necessary computation can be made efficient. In this section, we will discuss statistical modelling with a GP prior.

2.1 Gaussian processes and kernels

The key component of a GP is its covariance function, known as the *kernel*. In what follows we define kernel and GP.

Definition 1 (Kernel). *Let \mathcal{X} be a nonempty set. A symmetric function $k : \mathcal{X} \times \mathcal{X} \rightarrow \mathbb{R}$ is called positive definite kernel, or simply kernel, if for all $n = 1, 2, \dots$, $a_1, \dots, a_n \in \mathbb{R}$ and $\mathbf{x}_1, \dots, \mathbf{x}_n \in \mathcal{X}$,*

$$\sum_{i=1}^n \sum_{j=1}^n a_i a_j k(\mathbf{x}_i, \mathbf{x}_j) \geq 0. \quad (2.4)$$

Definition 2 (Gaussian Process). *Let \mathcal{X} be a non-empty set, $k : \mathcal{X} \times \mathcal{X} \rightarrow \mathbb{R}$ be a positive definite kernel, and $m : \mathcal{X} \rightarrow \mathbb{R}$ be a real-valued function. A random function $f : \mathcal{X} \rightarrow \mathbb{R}$ is a Gaussian Process with mean function m and kernel k , if, for any finite set $\mathbf{x}_i \in \mathcal{X}$ for $i = 1, \dots, n$, the random vector $\mathbf{f} = (f(\mathbf{x}_1), \dots, f(\mathbf{x}_n))^T$ follows multivariate Gaussian distribution $\mathbf{MVN}(\mathbf{m}, \mathbf{K})$ where $\mathbf{m} = (m(\mathbf{x}_1), \dots, m(\mathbf{x}_n))^T$ and \mathbf{K} is a $n \times n$ matrix with (i, j) -th element given by $k(\mathbf{x}_i, \mathbf{x}_j)$.*

For the rest of the paper, when a random function f follows a GP with a mean function m and a kernel k , we write $f \sim \text{GP}(m, k)$ and refer the matrix \mathbf{K} as a Gram matrix. GP is completely specified by its mean function and kernel. In other words, we can incorporate our belief about the regression function by choosing the corresponding mean function and kernel. In the absence of a prior belief, the mean function is often set to be zero, i.e., $m(x) = 0$ for all $x \in \mathcal{X}$. With this assumption, the kernel k defines a unique GP, and a specific choice of kernel leads to different assumptions on the corresponding process. For example, the squared exponential (SE) kernel (2.5) is one of the most widely used kernels, especially in machine learning,

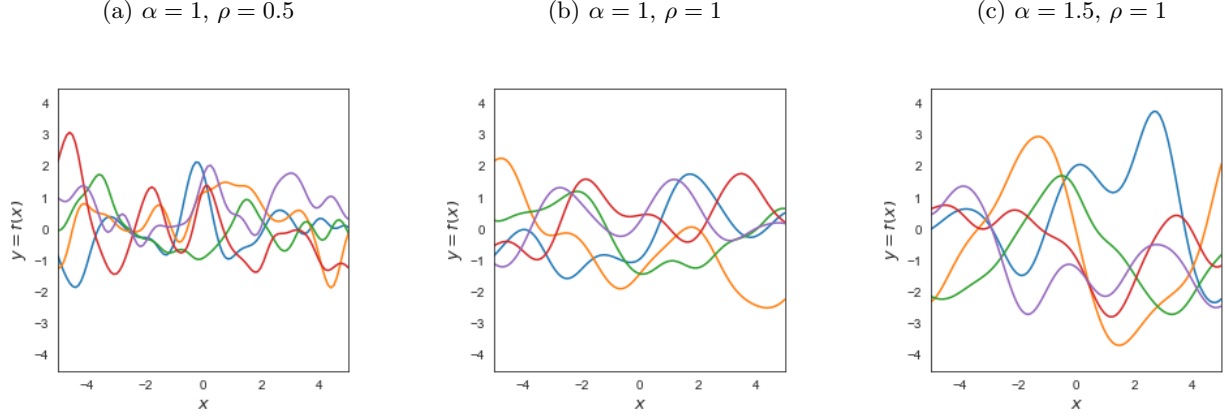


Figure 3: Sample paths from zero mean Gaussian process with 1-dimensional squared exponential kernel. Taking the middle (b) as reference, the left (a) has smaller length scale which makes the process more wiggly. Having a larger sample scale parameter as in (c) makes the average distance from the mean(0) bigger.

and associated with a very smooth process which has mean-square derivatives (Adler (1981, Chapter 2)) of all orders.

Example 1 (Squared exponential kernel). *Let $\mathcal{X} \subset \mathbb{R}^p$. For $\alpha > 0$ and $\rho > 0$, a squared exponential (SE) kernel $k_{se} : \mathcal{X} \times \mathcal{X} \rightarrow \mathbb{R}$ is defined by*

$$k_{se}(\mathbf{x}, \mathbf{x}') = \alpha^2 \exp\left(-\frac{\|\mathbf{x} - \mathbf{x}'\|^2}{2\rho^2}\right), \quad \mathbf{x}, \mathbf{x}' \in \mathcal{X}. \quad (2.5)$$

We refer unknown parameters in a kernel as hyper-parameters. In the example above, we have a scale parameter α and a length-scale parameter ρ . The values of these hyper-parameters also carry assumptions on the underlying process. See Figure 3 for a further demonstration of this. We show a few of the other popular kernels in machine learning and spatial statistics in Appendix A.1. For more comprehensive reviews on different classes of kernels, see Rasmussen and Williams (2006, Chapter 4) and Genton (2001) for example.

2.2 Statistical modelling with kernels

2.2.1 Sum kernels and main effect terms

Let us revisit the main effect model with 2 predictors specified in (2.1) and (2.2). Given two kernels $k_1 : \mathcal{X}_1 \times \mathcal{X}_1 \rightarrow \mathbb{R}$ and $k_2 : \mathcal{X}_2 \times \mathcal{X}_2 \rightarrow \mathbb{R}$, we assume $f_1 \sim \text{GP}(0, k_1)$ and $f_2 \sim \text{GP}(0, k_2)$. A nice property of kernels (see Appendix A.2) is that the sum of the given two valid kernels constitutes a new kernel. With the additional assumption that the constant term $a \sim N(0, \alpha_0^2)$ where $\alpha_0 > 0$, the overall function $f : \mathcal{X} \rightarrow \mathbb{R}$ with $\mathcal{X} = \mathcal{X}_1 \times \mathcal{X}_2$ follows $\text{GP}(0, k)$ where $k : \mathcal{X} \times \mathcal{X} \rightarrow \mathbb{R}$ is given by

$$k((\mathbf{x}_1, \mathbf{x}_2), (\mathbf{x}'_1, \mathbf{x}'_2)) = \alpha_0^2 + k_1(\mathbf{x}_1, \mathbf{x}'_1) + k_2(\mathbf{x}_2, \mathbf{x}'_2). \quad (2.6)$$

Note that the first term α_0^2 is also a positive definite kernel, known as a constant kernel (A.4), hence the function k can be seen as a sum of three positive definite kernels. The corresponding Gram matrix is given

by

$$\mathbf{K} = \alpha_0^2 \mathbf{1}\mathbf{1}_n^\top + \mathbf{K}_1 + \mathbf{K}_2 \quad (2.7)$$

where $\mathbf{1}\mathbf{1}_n^\top$ is a $n \times n$ matrix with all elements equal to 1, and \mathbf{K}_l is a Gram matrix with i, j -th element given by $k_l(\mathbf{x}_i, \mathbf{x}_j')$. We can generalize this to the case where with d predictors $\mathbf{x}_1, \dots, \mathbf{x}_d$.

Example 2 (Main effect kernel). *Let \mathcal{X}_l be a nonempty set and k_l be a positive definite kernel on $\mathcal{X}_l \times \mathcal{X}_l$ for $l = 1, \dots, d$. Let $\mathcal{X} = \mathcal{X}_1 \times \dots \times \mathcal{X}_d$. Given d predictors, the kernel that gives a main effect GP model is defined on $\mathcal{X} \times \mathcal{X}$ and given by*

$$k_{\text{main}}((\mathbf{x}_1, \dots, \mathbf{x}_d), (\mathbf{x}'_1, \dots, \mathbf{x}'_d)) = \alpha_0^2 + \sum_{l=1}^d k_l(\mathbf{x}_l, \mathbf{x}'_l), \quad \mathbf{x}_l, \mathbf{x}'_l \in \mathcal{X}_l. \quad (2.8)$$

2.2.2 Tensor product kernels and interaction effect terms

The interaction effect model (2.3) has an additional function term f_{12} . We put a zero mean GP prior on this, with its kernel $k : \mathcal{X} \times \mathcal{X} \rightarrow \mathbb{R}$ given by a tensor product of two kernels k_1 and k_2 . Formally, we have $k = k_1 \otimes k_2$ defined by $k((\mathbf{x}_1, \mathbf{x}_2), (\mathbf{x}'_1, \mathbf{x}'_2)) = k_1(\mathbf{x}_1, \mathbf{x}'_1)k_2(\mathbf{x}_2, \mathbf{x}'_2)$ where \otimes is a tensor product operator. Generalising this kernel to the case involving d predictors, we have the following definition.

Definition 3 (Tensor product kernel). *Let \mathcal{X}_l be a nonempty set and k_l be a positive definite kernel on $\mathcal{X}_l \times \mathcal{X}_l$ for $l = 1, \dots, d$. With $\mathcal{X} = \mathcal{X}_1 \times \dots \times \mathcal{X}_d$, a tensor product of $\{k_l\}_{l=1}^d$ is a kernel on $\mathcal{X} \times \mathcal{X}$ defined as*

$$(\otimes_{l=1}^d k_l)((\mathbf{x}_1, \dots, \mathbf{x}_d), (\mathbf{x}'_1, \dots, \mathbf{x}'_d)) = \prod_{l=1}^d k_l(\mathbf{x}_l, \mathbf{x}'_l), \quad \mathbf{x}_l, \mathbf{x}'_l \in \mathcal{X}_l. \quad (2.9)$$

Using the sum kernel for the main effect terms, and the tensor product kernel for the interaction effect term, we can specify the prior on the regression function f in (2.3) as $\text{GP}(0, k)$, where $k = \alpha^2 + k_1 + k_2 + k_1 \otimes k_2$ is defined by

$$k((\mathbf{x}_1, \mathbf{x}_2), (\mathbf{x}'_1, \mathbf{x}'_2)) = \alpha_0^2 + k_1(\mathbf{x}_1, \mathbf{x}'_1) + k_2(\mathbf{x}_2, \mathbf{x}'_2) + k_1(\mathbf{x}_1, \mathbf{x}'_1)k_2(\mathbf{x}_2, \mathbf{x}'_2). \quad (2.10)$$

The corresponding Gram matrix can be written as

$$\mathbf{K} = \alpha_0^2 \mathbf{1}\mathbf{1}_n^\top + \mathbf{K}_1 + \mathbf{K}_2 + \mathbf{K}_1 \circ \mathbf{K}_2 \quad (2.11)$$

where \circ is the element-wise product operator.

2.2.3 ANOVA decomposition kernel

When including interaction terms in a model, it is a common practice to include both the main terms and any lower order interaction terms. In this section we introduce a special class of additive kernels, known as the ANOVA decomposition kernel, that can naturally take this into consideration. For a model with d predictors, we define a saturated ANOVA decomposition kernel as follows.

Definition 4 (Saturated ANOVA decomposition kernel). *Let \mathcal{X}_l be a nonempty set and k_l be a positive definite kernel on $\mathcal{X}_l \times \mathcal{X}_l$ for $l = 1, \dots, d$. With $\mathcal{X} = \mathcal{X}_1 \times \dots \times \mathcal{X}_d$, the saturated ANOVA decomposition*

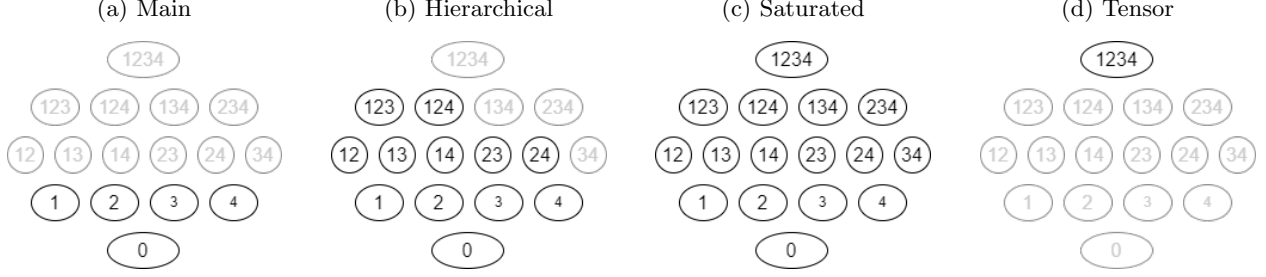


Figure 4: Visualisation of ANOVA decomposition kernels (Panel (a),(b) and (c)) and a tensor product kernel (Panel (d)) with $d = 4$ dimensional covariates. The term 0 in the panels refers to the constant term, and the terms 1 to 4 refers to main effect term that corresponds to k_l for $l = 1, \dots, 4$. The remaining terms are interaction effect terms, e.g., the term 123 models the three-way interaction effect involving the covariates $\mathbf{x}_1, \mathbf{x}_2$ and \mathbf{x}_3 . Panel (b) is an example of a Hierarchical ANOVA decomposition kernel. Adding the term 34 to this example gives another example of such kernel. If we are to include the term 134 and/or 234, the term 34 should also be added in order to ensure a hierarchical structure.

kernel $k_{s-anova} : \mathcal{X} \times \mathcal{X} \rightarrow \mathbb{R}$ is given by:

$$k_{s-anova}((\mathbf{x}_1, \dots, \mathbf{x}_l), (\mathbf{x}'_1, \dots, \mathbf{x}'_l)) = \prod_{l=1}^d (1 + k_l(\mathbf{x}_l, \mathbf{x}'_l)), \quad \mathbf{x}_l, \mathbf{x}'_l \in \mathcal{X}_l. \quad (2.12)$$

The (saturated) ANOVA decomposition kernel was first introduced by Stitson et al. (1999) in the context of Support Vector Machines. It borrows the idea of an ANOVA decomposition of a function in a Reproducing Kernel Hilbert Space (RKHS) (Wahba et al., 1995). This kernel has 2^d terms, including a constant term 1, all of the base kernels, the d -th order interaction term and any lower order interaction terms. The kernel given by (2.10) is in fact this class of kernel, if we set $\alpha_0^2 = 1$. It can also be seen as a special case of tensor product kernels, by treating $\tilde{k}(\mathbf{x}_l, \mathbf{x}'_l) = 1 + k_l(\mathbf{x}_l, \mathbf{x}'_l)$ as one kernel. In contrast to the saturated ANOVA decomposition kernel, a GP model with a tensor product kernel in its simplest form given by Definition 3 only includes the highest interaction term. As we will see in the following sections, this may lead to a poor fit, and cause difficulty in interpretation of the fitted model. The saturated ANOVA kernel, however, assumes the highest complexity given a set of base kernels, which may be an over-fit to the data.

Therefore, we introduce another class of ANOVA decomposition kernels, called the *hierarchical decomposition ANOVA kernel*. This kernel includes a constant 1, all main terms k_l for $l = 1, \dots, d$, and any interaction terms of any orders constructed using tensor product kernels. Additionally, this kernel must have a hierarchical structure, meaning that if we include any p -th order interaction terms, any lower order interaction terms involving any covariates used in the p -th order interaction terms must also be included. The smallest kernel in this class is the main effect kernel given by (2.8), and the largest kernel is simply the saturated ANOVA decomposition kernel. Figure 4 illustrates the differences between the kernels discussed in this section with $d = 4$. It is worth noting that there are many hierarchical ANOVA kernels, and Figure 4b shows one such example.

2.3 Centring of kernels

Gaussian process paths may be arbitrary positioned, in which case, centring of kernels can be applied. A positive definite kernel can be centred by the following.

Definition 5 (Centred kernel). *Let P be a probability distribution over a non empty set \mathcal{X} and $X, X' \sim P$*

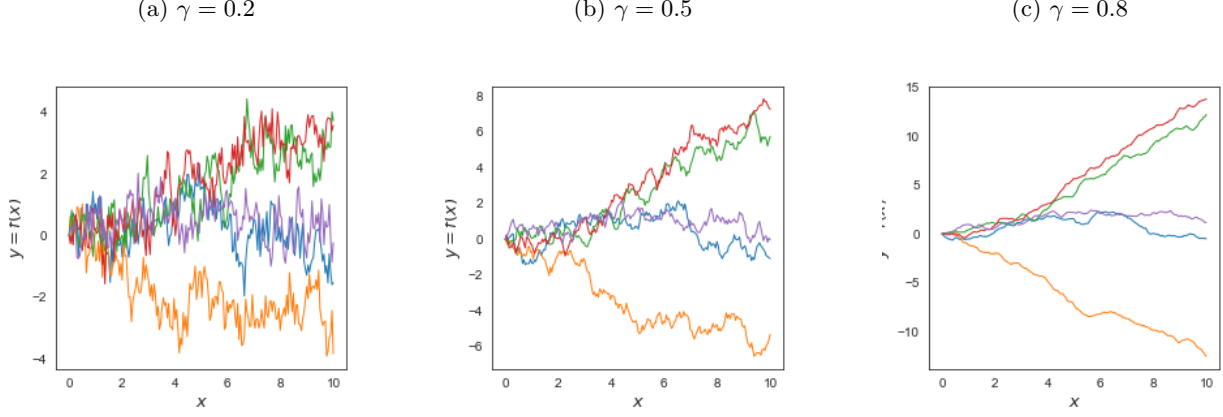


Figure 5: Sample paths from fBM kernel given in (2.15) with different values for Hurst coefficient γ .

are independent. Any kernel $k : \mathcal{X} \times \mathcal{X} \rightarrow \mathbb{R}$ may be centred by

$$k_{cent}(\mathbf{x}, \mathbf{x}') = \mathbb{E}_P [k(\mathbf{x}, \mathbf{x}') - k(\mathbf{x}, X) - k(\mathbf{x}', X') + k(X, X')], \quad \mathbf{x}, \mathbf{x}' \in \mathcal{X}. \quad (2.13)$$

A kernel centred by the above is positive definite. We provide a proof in A.5. In practice, we can use the empirical distribution of data $\mathbf{x}_1, \dots, \mathbf{x}_n$ to approximate the unknown P , i.e.,

$$k_{cent}(\mathbf{x}, \mathbf{x}') = k(\mathbf{x}, \mathbf{x}') - \frac{1}{n} \sum_{i=1}^n k(\mathbf{x}, \mathbf{x}_i) - \frac{1}{n} \sum_{j=1}^n k(\mathbf{x}', \mathbf{x}_j) + \frac{1}{n^2} \sum_{i=1}^n \sum_{j=1}^n k(\mathbf{x}_i, \mathbf{x}_j). \quad (2.14)$$

This ensures the sum of the function f evaluated at $\mathbf{x}_1, \dots, \mathbf{x}_n$ to be zero, i.e., $\sum_{i=1}^n f(\mathbf{x}_i) = 0$. Given a positive semi-definite Gram matrix \mathbf{K} , the Gram matrix after empirical centring, $\mathbf{K}^{(c)}$, can be computed using a centring matrix $\mathbf{C} = \mathbf{I}_n - \frac{1}{n} \mathbf{1}\mathbf{1}^\top$, by $\mathbf{K}^{(c)} = \mathbf{C}\mathbf{K}\mathbf{C}$. This means that all columns and rows of the matrix sum to 0. centring of a kernel plays a key role in constructing an efficient Kronecker approach for additiveGP models with hierarchical ANOVA decomposition kernels as shown in Section 3.

centring example with fractional Brownian motion kernel

We will illustrate centring of kernels using fractional Brownian Motion (fBM) kernel.

Example 3 (fractional Brownian motion kernel). Let $\mathcal{X} \subset \mathbb{R}^p$ be a nonempty set. For $\alpha > 0$ and $0 < \gamma < 1$, the fractional Brownian motion kernel $k_{fBM_\gamma} : \mathcal{X} \times \mathcal{X} \rightarrow \mathbb{R}$ is defined by

$$k_{fBM_\gamma}(\mathbf{x}, \mathbf{x}') = \frac{\alpha^2}{2} (\|\mathbf{x}\|^{2\gamma} + \|\mathbf{x}'\|^{2\gamma} - \|\mathbf{x} - \mathbf{x}'\|^{2\gamma}), \quad \mathbf{x}, \mathbf{x}' \in \mathcal{X} \quad (2.15)$$

The parameter γ , known as the Hurst coefficient, determines the roughness of the process. A smaller value of the Hurst coefficient is associated with rougher sample paths (see Figure 5). With $\gamma = 0.5$, we have standard Brownian motion. From Figure 5, we notice $f(0) = 0$ for all paths, which may be undesirable for the problems we consider in the paper. To avoid this, a fBM kernel can be centred.

Example 4 (centred fractional Brownian Motion kernel). Applying (2.14) to the fBM kernel (2.15), we

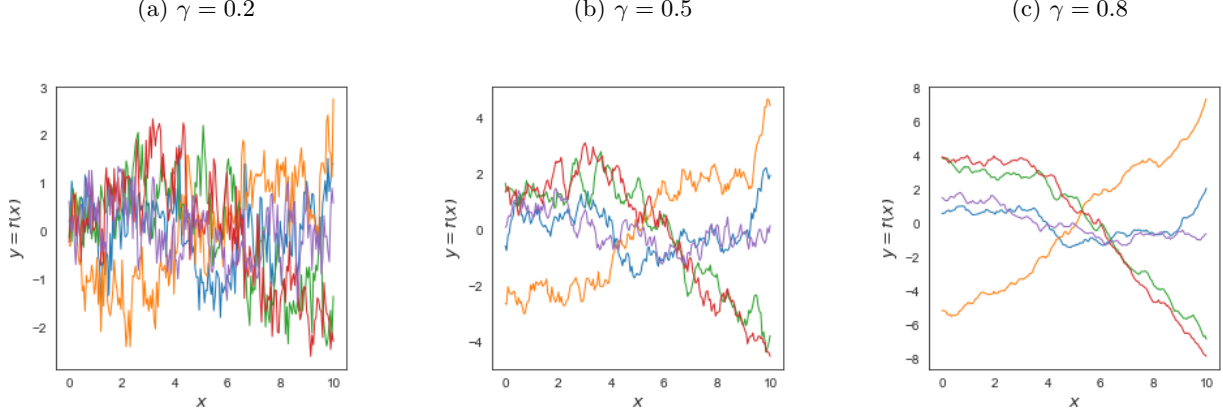


Figure 6: Sample paths from centred fBM kernels (2.16) with different values for Hurst coefficient γ .

have

$$k_{cfBM_\gamma}(\mathbf{x}, \mathbf{x}') = \frac{\alpha^2}{2n^2} \sum_{i=1}^n \sum_{j=1}^n (||\mathbf{x} - \mathbf{x}_i||^{2\gamma} + ||\mathbf{x}' - \mathbf{x}_j||^{2\gamma} - ||\mathbf{x} - \mathbf{x}'||^{2\gamma} - ||\mathbf{x}_i - \mathbf{x}_j||^{2\gamma}) \quad (2.16)$$

The difference between non-centred and centred paths of standard Brownian motion is illustrated in Figure 5 and 6. In this paper, we will always center fBM kernels with respect to the empirical distribution.

Another issues with the fBM kernel in (2.15) is its roughness. In contrast to a GP with SE kernel, fractional Brownian motion paths are differentiable nowhere, hence they may be too rough to be used in many examples. To remedy this, we introduce a squared kernel.

Definition 6 (Squared kernel). *Let \mathcal{X} be a non-empty set. Given a kernel $k : \mathcal{X} \times \mathcal{X} \rightarrow \mathbb{R}$, squared kernel is a function $k_{sq} : \mathcal{X} \times \mathcal{X} \rightarrow \mathbb{R}$ given by*

$$k_{sq}(\mathbf{x}, \mathbf{x}') = \sum_{i=1}^n k(\mathbf{x}, \mathbf{x}_i)k(\mathbf{x}', \mathbf{x}_i), \quad \mathbf{x}, \mathbf{x}' \in \mathcal{X}. \quad (2.17)$$

As this kernel consists of products and sums of kernels, it is a positive definite kernel. The corresponding Gram matrix is given by $\mathbf{K}_{sq} = \mathbf{K}\mathbf{K}$. If we use the empirically centred kernel in the construction, the resulting Gram matrix $\mathbf{K}_{sq}^{(c)} = \mathbf{K}^{(c)}\mathbf{K}^{(c)}$ is still empirically centred, as we have,

$$\mathbf{K}_{sq}^{(c)} \mathbf{1} = \mathbf{K}^{(c)} \left(\mathbf{K}^{(c)} \mathbf{1} \right) = \mathbf{K}^{(c)} \mathbf{0} = \mathbf{0}. \quad (2.18)$$

This kernel is shown useful in the previous work by Bergsma (2020), Jamil (2018), and Jamil and Bergsma (2020) in the context of iprior, which has close connection to GPs and kernel methods. From Figure 6, we can see that GP paths wit squared (and centred) γ -fBM kernels are much smoother. In fact, the smoothness properties of GP paths with fBM kernel and squared fBM kernel can be discussed in terms of Hölder condition. While the realisations from the former are known to be a.s. Hölder of any order less than γ (see Embrechts and Maejima (2002) for example), the latter is Hölder of order 2γ . Bergsma (2020) discusses the smoothness properties of fBM paths and squared fBM path using different concepts of smoothness, including Hölder condition and regularity.

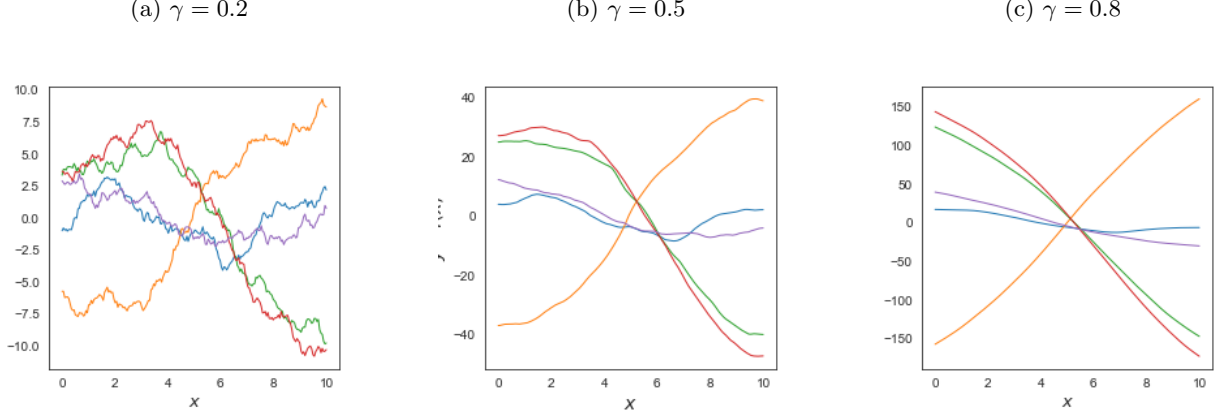


Figure 7: Sample paths from square-summed fBM kernels constructed using (2.16) (2.17) with different values for Hurst coefficient γ .

2.4 Estimation and inference

Let us revisit the regression model in (2.1) where we assume a zero-mean GP prior on f and i.i.d error. With $\mathbf{y} = (y_1, \dots, y_n)^\top$ and \mathbf{X} being a data matrix gathering covariates from all observations, we have:

$$\mathbf{y}|\mathbf{X} \sim \text{MVN}_n(\mathbf{0}, \mathbf{K} + \sigma^2 \mathbf{I}). \quad (2.19)$$

The following section discusses the posterior distribution and the estimation of the hyper-parameters.

2.4.1 Posterior

For Gaussian likelihood, GP is a conjugate prior, i.e., the posterior is also a GP. Specifically, we have $f|\mathbf{y}, \mathbf{X} \sim \text{GP}(\bar{m}, \bar{k})$ with the mean function $\bar{m} : \mathcal{X} \rightarrow \mathbb{R}$ and the kernel $\bar{k} : \mathcal{X} \times \mathcal{X} \rightarrow \mathbb{R}$ given by

$$\bar{m}(\mathbf{x}) = \mathbf{k}(\mathbf{x})^\top (\mathbf{K} + \sigma^2 \mathbf{I})^{-1} \mathbf{y}, \quad \mathbf{x} \in \mathcal{X} \quad (2.20)$$

$$\bar{k}(\mathbf{x}, \mathbf{x}') = k(\mathbf{x}, \mathbf{x}') - \mathbf{k}(\mathbf{x})^\top (\mathbf{K} + \sigma^2 \mathbf{I})^{-1} \mathbf{k}(\mathbf{x}'), \quad \mathbf{x}, \mathbf{x}' \in \mathcal{X} \quad (2.21)$$

where $\mathbf{k}(\mathbf{x}) = (k(\mathbf{x}_1, \mathbf{x}), \dots, k(\mathbf{x}_n, \mathbf{x}))^\top$ for $\mathbf{x} \in \mathcal{X}$. See Appendix A.3 for the derivation. Figure 8 shows an example with a one-dimensional GP with SE kernel. The posterior given by (2.20) and (2.21) may more commonly be discussed in connection to prediction problems. In fact, given a new point \mathbf{x}^* the posterior predictive distribution over $f(\mathbf{x}^*)$ is Gaussian with mean $\bar{m}(\mathbf{x}^*)$ and variance $\bar{k}(\mathbf{x}^*, \mathbf{x}^*)$.

2.4.2 Decomposition of the posterior under additive models and interpretability

When the kernel and the regression function have an additive structure, i.e., $k_{all} = \sum_{j=1}^J k_j$ and $f_{all} = \sum_{j=1}^J f_j$ where each k_j is defined on $\mathcal{D}_j \times \mathcal{D}_j$ with a nonempty set \mathcal{D}_j and $f_j \sim \text{GP}(0, k_j)$, the posterior mean and kernel for the j -th component f_j can also be decomposed as

$$\bar{m}_j(\mathbf{x}_j) = \mathbf{k}_j(\mathbf{x}_j)^\top (\mathbf{K}_{all} + \sigma^2 \mathbf{I}_n)^{-1} \mathbf{y}, \quad \mathbf{x}_j \in \mathcal{D}_j \quad (2.22)$$

$$\bar{k}_j(\mathbf{x}_j, \mathbf{x}'_j) = \bar{k}_j(\mathbf{x}_j, \mathbf{x}'_j) - \mathbf{k}_j(\mathbf{x}_j)^\top (\mathbf{K}_{all} + \sigma^2 \mathbf{I}_n)^{-1} \mathbf{k}_j(\mathbf{x}'_j), \quad \mathbf{x}_j, \mathbf{x}'_j \in \mathcal{D}_j \quad (2.23)$$

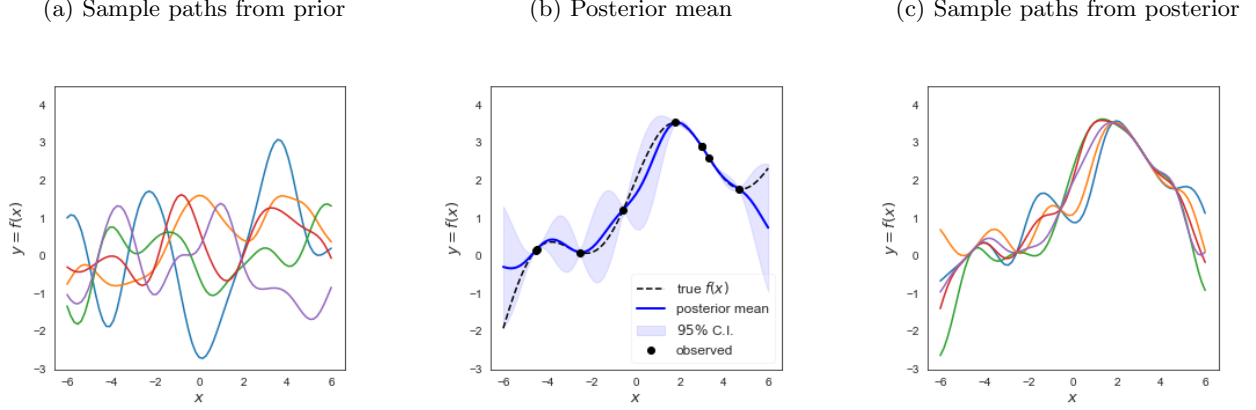


Figure 8: Example of regression/curve fitting in 1 dimension with Gaussian process prior. Consider that we have a sample of size 7 (from a true function, $f(x) = 2 + \frac{2}{5}x - \frac{1}{20}x^2 + \sin x$). The prior is a GP with SE kernel with $\alpha = 1$ and $\rho = 1$. The panel (a) shows sample paths from the prior GP and (b) shows the posterior mean with 95% confidence interval together with the observations and the true function. Random sample paths drawn from the posterior are shown in (c).

for $j = 1, 2, \dots, J$ and J denoting the number of terms. Note that here we treat any tensor product kernel as one kernel, e.g. the j -th term can be $k_j(\mathbf{x}_j, \mathbf{x}'_j) = k_l(\mathbf{x}_l, \mathbf{x}'_l)k_m(\mathbf{x}_m, \mathbf{x}'_m)$ with $\mathbf{x}_j = (\mathbf{x}_l, \mathbf{x}_m)$ and $\mathcal{D}_j = \mathcal{X}_l \times \mathcal{X}_m$. As discussed in Plate (1999) and Duvenaud et al. (2011), one effective way to interpret an additive GP model is to visualise each function contributing to the model. Using this decomposition, it is possible to visually understand the main effects of each covariate, as well as any interaction effects by plotting the posterior mean of the function with a specific kernel. We will illustrate this with a real-world application in Section 4.

2.4.3 Hyper-parameter estimation and model comparison

The fully Bayesian way to estimate hyper-parameters, including parameters in the kernels and the variance in the error term σ^2 , is to put priors on hyper-parameters, in which case we most typically resort to Markov chain Monte Carlo (MCMC). Alternatively, we can use Empirical Bayes, where the parameters are estimated by maximising the log marginal likelihood denoted by $p(\mathbf{y}) = \int p(\mathbf{y}|\mathbf{f})p(\mathbf{f}|\mathbf{X}, \mathbf{y})$. With Gaussian likelihood, the log marginal likelihood equals

$$\log p(\mathbf{y}) = -\frac{1}{2}\mathbf{y}^\top (\mathbf{K} + \sigma^2 \mathbf{I}_n)^{-1} \mathbf{y} - \frac{1}{2} \log |\mathbf{K} + \sigma^2 \mathbf{I}_n| - \frac{n}{2} \log 2\pi. \quad (2.24)$$

Since the marginal likelihood penalises model complexity, i.e., more complex model does not necessarily lead to larger marginal likelihood (MacKay, 1995; Murray & Ghahramani, 2005), it can be used for comparing different models.

3 Efficient computation using Kronecker methods for multidimensional grid data

The evaluation of the log marginal likelihood (2.24) and the posterior mean (2.20) and covariance (2.21) involves the $n \times n$ marginal covariance matrix $\mathbf{K} + \sigma^2 \mathbf{I}$, which has a computational time complexity of $O(n^3)$ and storage requirements of $O(n^2)$. However, when a multidimensional grid structure is present in

the data, these computations can be made more efficient. Unlike other scalable methods such as subset of data, Nyström methods (Williams & Seeger, 2001), inducing points, and sparse variational methods (e.g., Titsias (2009)), the Kronecker approach does not perform approximation, but rather exploits the structure of the data to efficiently evaluate and store the key components required for estimation and inference. The primary component of Kronecker methods is a Gram matrix represented in the form of a Kronecker product. Appendix B.1 introduces the Kronecker product and its key properties. Revisiting the regression model example (2.1), if \mathbf{x}_1 and \mathbf{x}_2 form a two-dimensional grid, we can rewrite the model equation as

$$y_{i,j} = f(\mathbf{x}_{1i}, \mathbf{x}_{2j}) + \epsilon_{i,j} \quad (3.1)$$

where $y_{i,j}$ is the response from the i -th station at time j with $i = 1, \dots, n_1$, $j = 1, \dots, n_2$ and $n = n_1 \times n_2$. We write $\mathbf{y} = (y_{1,1}, \dots, y_{1,n_2}, \dots, y_{n_1,1}, \dots, y_{n_1,n_2})$ and define $\boldsymbol{\epsilon}$ similarly. The main effect and interaction effect models in (2.2) and (2.3) then can be specified by

$$f(\mathbf{x}_{1i}, \mathbf{x}_{2j}) = a + f_1(\mathbf{x}_{1i}) + f_2(\mathbf{x}_{2j}) \quad (3.2)$$

$$f(\mathbf{x}_{1i}, \mathbf{x}_{2j}) = a + f_1(\mathbf{x}_{1i}) + f_2(\mathbf{x}_{2j}) + f_{12}(\mathbf{x}_{1i}, \mathbf{x}_{2j}). \quad (3.3)$$

If we use the same prior as the previous model with $\alpha_0 = 1$, we have $\mathbf{y} \sim \text{MVN}_n(\mathbf{0}, \mathbf{K} + \sigma^2 \mathbf{I}_n)$ with the Gram matrix for each model given by

$$\mathbf{K} = \mathbf{1}\mathbf{1}_{n_1}^\top \otimes \mathbf{1}\mathbf{1}_{n_2}^\top + \mathbf{K}_1 \otimes \mathbf{1}\mathbf{1}_{n_2}^\top + \mathbf{1}\mathbf{1}_{n_1}^\top \otimes \mathbf{K}_2. \quad (3.4)$$

for the main effect model, and

$$\begin{aligned} \mathbf{K} &= (\mathbf{1}\mathbf{1}_{n_1}^\top + \mathbf{K}_1) \otimes (\mathbf{1}\mathbf{1}_{n_2}^\top + \mathbf{K}_2) \\ &= \mathbf{1}\mathbf{1}_{n_1}^\top \otimes \mathbf{1}\mathbf{1}_{n_2}^\top + \mathbf{K}_1 \otimes \mathbf{1}\mathbf{1}_{n_2}^\top + \mathbf{1}\mathbf{1}_{n_1}^\top \otimes \mathbf{K}_2 + \mathbf{K}_1 \otimes \mathbf{K}_2 \end{aligned} \quad (3.5)$$

for the interaction effect models, where \otimes is a Kronecker product operator.

The Kronecker method has been used and proven useful for efficient implementation of GP models (e.g. Saatçi (2012, Chapter 5), Groot et al. (2014) Wilson et al. (2014) and Flaxman et al. (2015)). However, so far, only tensor product kernels were considered in the papers. This corresponds to having only the interaction term, i.e., only the last term in (3.5) and (3.5), if the base kernels do not have an additive structure. In this paper, we extend the use of Kronecker methods to a model with a saturated ANOVA kernel, and also to a hierarchical ANOVA kernel. The former is a type of a tensor product kernel, thus the methods discussed in the literature directly applies. The latter is not straight-forward, however, we show that, by using centred kernel, we can still benefit from Kronecker algebra.

3.1 Kronecker methods for saturated ANOVA decomposition kernel

Now let us assume that we have d -dimensional grid structure in the predictors. Let n_l denote the length of the l -th level predictor \mathbf{x}_l for $l = 1, \dots, d$. We have a response vector \mathbf{y} of length $n = \prod_{l=1}^d n_l$. If we use the saturated ANOVA decomposition kernel (2.12), the Gram matrix can be written as

$$\mathbf{K} = \bigotimes_{l=1}^d \tilde{\mathbf{K}}_l \quad (3.6)$$

where $\tilde{\mathbf{K}}_l = (\mathbf{1}\mathbf{1}_{n_l}^\top + \mathbf{K}_l)$ and $\mathbf{K}_l = \{k_{l,(i,j)}\}_{n_l \times n_l}$ with $k_{l,(i,j)} = k_l(\mathbf{x}_{l,i}, \mathbf{x}_{l,j})$. Using the eigendecomposition, $\tilde{\mathbf{K}}_l = \tilde{\mathbf{Q}}_l \tilde{\mathbf{\Lambda}}_l \tilde{\mathbf{Q}}_l^\top$ and the properties of Kronecker product (see Appendix B.1 and B.2), we can write

$$\mathbf{K} + \sigma^2 \mathbf{I}_n = \left(\bigotimes_{l=1}^d \tilde{\mathbf{Q}}_l \right) \left(\bigotimes_{l=1}^d \tilde{\mathbf{\Lambda}}_l + \sigma^2 \mathbf{I}_n \right) \left(\bigotimes_{l=1}^d \tilde{\mathbf{Q}}_l \right)^\top. \quad (3.7)$$

Note that $\tilde{\mathbf{Q}} := \left(\bigotimes_{l=1}^d \tilde{\mathbf{Q}}_l \right)$ is orthonormal by (B.13) and $\tilde{\mathbf{\Lambda}} := \left(\bigotimes_{l=1}^d \tilde{\mathbf{\Lambda}}_l + \sigma^2 \mathbf{I}_n \right)$ is diagonal. The multiplication of the inverted matrix and a vector \mathbf{v} can be expressed as

$$(\mathbf{K} + \sigma^2 \mathbf{I}_n)^{-1} \mathbf{v} = \left(\bigotimes_{l=1}^d \tilde{\mathbf{Q}}_l \right) \left(\bigotimes_{l=1}^d \tilde{\mathbf{\Lambda}}_l + \sigma^2 \mathbf{I}_n \right)^{-1} \left(\bigotimes_{l=1}^d \tilde{\mathbf{Q}}_l \right)^\top \mathbf{v}. \quad (3.8)$$

The inversion of the middle diagonal matrix can be done by simply inverting its diagonal elements. The log determinant is given by

$$\log |\mathbf{K} + \sigma^2 \mathbf{I}| = \sum_{l=1}^n \log(\lambda_l + \sigma^2) \quad (3.9)$$

where $\boldsymbol{\lambda} = \text{diag}(\tilde{\mathbf{\Lambda}})$. This approach has computational complexity of $O(\sum_{l=1}^d n_l^3)$ or $O(n \sum_{l=1}^d n_l)$, associated with the cost of the eigen-decomposition of each Gram matrix or the Kronecker product matrix-vector multiplication, respectively. This is much less than the crude approach that costs $O(n^3)$. More detailed analysis of computational complexity is discussed in Section 3.3. The use of this approach is limited to when we have a tensor product kernel, including the saturated ANOVA kernel. The former can be implemented by replacing $\tilde{\mathbf{K}}_l$ with \mathbf{K}_l . As mentioned previously using a tensor product kernel implies including only the interaction term of the highest order. This may be problematic in many applications where assessing the effect of each predictor is needed. Using ANOVA kernel, on the other hand, means that we assume a saturated model, which could often overfit the data.

3.2 Kronecker methods for nonsaturated hierarchical ANOVA decomposition kernel

In this section, we show that the Kronecker product structure can be exploited for efficient computation even when we have a more general structure in the kernel, such as (3.4), by using an empirically centred kernel (2.14). Consider a hierarchical ANOVA kernel for data with a d -dimensional grid structure. Let us now assume that we have m terms in our additive kernel where $1 + d \leq m \leq 2^d$. The corresponding Gram matrix \mathbf{K} then also involves addition of m matrices \mathbf{M}_p for $p = 1, \dots, m$, i.e., we have

$$\mathbf{K} = \sum_{p=1}^m \mathbf{M}_p \quad (3.10)$$

where

$$\mathbf{M}_p = \left(\bigotimes_{l=1}^d \mathbf{B}_l \right) \text{ where } \mathbf{B}_l = \begin{cases} \mathbf{K}_l^{(c)}, & \text{if } k_l^{(c)} \text{ is involved in the } p\text{-th term} \\ \mathbf{1}\mathbf{1}_{n_l}^\top, & \text{otherwise.} \end{cases} \quad (3.11)$$

For this class of Gram matrices, we have the following lemma.

Lemma 1. A matrix \mathbf{K} of the form $\mathbf{K} = \sum_{p=1}^m \mathbf{M}_p$ has the following decomposition:

$$\mathbf{K} = \left(\bigotimes_{l=1}^d \mathbf{Q}_l^{(c)} \right) \mathbf{D} \left(\bigotimes_{l=1}^d \mathbf{Q}_l^{(c)} \right)^\top \quad (3.12)$$

where $\mathbf{Q}_l^{(c)}$ is orthonormal matrix whose columns consist of eigenvectors of $\mathbf{K}_l^{(c)}$ and \mathbf{D} is diagonal.

Proof. From Lemma 3 (see A.19 and A.22), for $l = 1, \dots, d$, we have:

$$\mathbf{K}_l^{(c)} = \mathbf{Q}_l^{(c)} \mathbf{\Lambda}_l^{(c)} \mathbf{Q}_l^{(c)\top} \quad (3.13)$$

$$\mathbf{1}\mathbf{1}_{n_l}^\top = \mathbf{Q}_l^{(c)} \mathbf{A}_l \mathbf{Q}_l^{(c)\top} \quad (3.14)$$

where (3.13) is an eigen-decomposition of a centred matrix $\mathbf{K}_l^{(c)}$ i.e., $\mathbf{Q}_l^{(c)}$ is orthonormal, $\mathbf{\Lambda}_l^{(c)}$ is diagonal (see A.20 and A.21) and \mathbf{A}_l is a $n_l \times n_l$ matrix with $\mathbf{A}_{1,1} = n_l$ and 0 everywhere else. Then using the mixed product property of Kronecker products, we can decompose \mathbf{M}_p as

$$\mathbf{M}_p = \bigotimes_{l=1}^d \mathbf{Q}_l^{(c)} \bigotimes_{l=1}^d \mathbf{D}_{pl} \bigotimes_{l=1}^d \mathbf{Q}_l^{(c)\top} \quad (3.15)$$

where

$$\mathbf{D}_{pl} = \begin{cases} \mathbf{\Lambda}_l^{(c)} & \text{if } k_l^{(c)} \text{ is involved in the } p\text{-th term} \\ \mathbf{A}_l & \text{otherwise.} \end{cases} \quad (3.16)$$

Let $\mathbf{D}_p = \bigotimes_{l=1}^d \mathbf{D}_{pl}$, which is a matrix with all off-diagonal elements 0. We have

$$\begin{aligned} \mathbf{K} = \sum_{p=1}^m \mathbf{M}_p &= \sum_{p=1}^m \left(\bigotimes_{l=1}^d \mathbf{Q}_l^{(c)} \mathbf{D}_p \bigotimes_{l=1}^d \mathbf{Q}_l^{(c)\top} \right) \\ &= \bigotimes_{l=1}^d \mathbf{Q}_l^{(c)} \left(\sum_{p=1}^m \mathbf{D}_p \right) \bigotimes_{l=1}^d \mathbf{Q}_l^{(c)\top} \end{aligned}$$

It is easy to see that the middle matrix $\mathbf{D} := \sum_{p=1}^m \mathbf{D}_p$ is diagonal. □

With this decomposition, we can write

$$\mathbf{K} + \sigma^2 \mathbf{I}_n = \mathbf{Q} (\mathbf{D} + \sigma^2 \mathbf{I}_n) \mathbf{Q}^\top \quad (3.17)$$

Noting that with $\sigma > 0$, all diagonal elements of $\mathbf{D} + \sigma^2 \mathbf{I}_n$ are positive, hence the overall matrix is invertible. The matrix inversion and log determinant can be obtained in the same way as discussed in the section above for the saturated ANOVA decomposition kernel.

Example 5 (Example of the Kronecker method for a hierarchical ANOVA kernel with $d = 2$). Consider a model specified by (3.1) and (3.2), i.e., the main effect model for two-dimensional grid data. If we use centred kernels, the Gram matrix given by (3.4) can be written as

$$\mathbf{K} = \mathbf{1}\mathbf{1}_{n_1}^\top \otimes \mathbf{1}\mathbf{1}_{n_2}^\top + \mathbf{K}_1^{(c)} \otimes \mathbf{1}\mathbf{1}_{n_2}^\top + \mathbf{1}\mathbf{1}_{n_1}^\top \otimes \mathbf{K}_2^{(c)}$$

and can be decomposed as

$$\begin{aligned} \mathbf{K} &= \mathbf{Q}_1^{(c)} \mathbf{A}_1 \mathbf{Q}_1^{(c)\top} \otimes \mathbf{Q}_2^{(c)} \mathbf{A}_2 \mathbf{Q}_2^{(c)\top} + \mathbf{Q}_1^{(c)} \mathbf{\Lambda}_1 \mathbf{Q}_1^{(c)\top} \otimes \mathbf{Q}_2^{(c)} \mathbf{A}_2 \mathbf{Q}_2^{(c)\top} + \mathbf{Q}_1^{(c)} \mathbf{A}_1 \mathbf{Q}_1^{(c)\top} \otimes \mathbf{Q}_2^{(c)} \mathbf{\Lambda}_2 \mathbf{Q}_2^{(c)\top} \\ &= \left(\mathbf{Q}_1^{(c)} \otimes \mathbf{Q}_2^{(c)} \right) (\mathbf{A}_1 \otimes \mathbf{A}_2 + \mathbf{\Lambda}_1 \otimes \mathbf{A}_2 + \mathbf{A}_1 \otimes \mathbf{\Lambda}_2) \left(\mathbf{Q}_1^{(c)} \otimes \mathbf{Q}_2^{(c)} \right)^\top. \end{aligned} \quad (3.18)$$

Thus far, we have restricted the prior variance of the constant term a in (3.2) and (3.3) to be 1, which corresponds with the first term of the Gram matrix being $\mathbf{1}_{n_1}^\top \otimes \mathbf{1}_{n_1}^\top$. Lifting this assumption is straightforward. If the prior variance is α_0^2 , the decomposition of the corresponding Gram matrix can be expressed in the same way as (3.18) with the first term of the middle matrix multiplied by α_0^2 .

3.3 Computational complexity and space requirement

Kronecker methods significantly reduce the cost of computing the log determinant of the matrix $\mathbf{K} + \sigma^2 \mathbf{I}$, and solving the linear system $(\mathbf{K} + \sigma^2 \mathbf{I})^{-1} \mathbf{v}$, which usually has $O(n^3)$ when \mathbf{K} is an $n \times n$ Gram matrix. As seen in (3.8) and (3.9), the key operations are eigendecomposition to get eigenvalues and a matrix of eigenvectors, and matrix-vector multiplication involving Kronecker products. With a Kronecker product structure, eigendecomposition is applied to each \mathbf{K}_l of size $n_l \times n_l$ individually, which has $O(n_l^3)$ complexity. The total cost for the eigendecomposition of \mathbf{K} then reduces to $O(\sum_{l=1}^d n_l^3)$, which is dominated by the largest of n_l . The second component is a matrix-vector multiplication in $(\bigotimes_{l=1}^d \mathbf{Q}_l^\top) \mathbf{v}$. A matrix-vector multiplication of an $n \times n$ matrix and a vector of length n usually requires $O(n^2)$ operations. Using the algorithm provided in Saatçi (2012, Chapter 5) and Wilson et al. (2014), this Kronecker product matrix-vector multiplication takes $O(n \sum_{l=1}^d n_l)$ which is much less than the usual $O(n^2)$. Once we have eigenvalues of all sub-Gram matrices \mathbf{K}_l , computing the log-determinant has an additional cost of $O(n)$. The storage requirement reduces from $O(n^2)$ to $O(\sum_{l=1}^d n_l^2)$ which is associated with storing matrices $\mathbf{Q}_1, \dots, \mathbf{Q}_d$. Previous work by Saatçi (2012) and Wilson et al. (2014) explored the use of the Kronecker method in Gaussian process regression and demonstrated improved computational time through simulation studies. Our approach, which shares the same key factors determining computational cost (namely, eigendecomposition of Gram matrices and matrix-vector multiplication), is expected to yield similar computational gains.

4 Application to NO₂ concentration in London

We apply the proposed method to analyse the dataset of hourly-measured concentrations of nitrogen dioxide (NO₂) in London collected before and after the first COVID-19 lockdown in the UK. NO₂ is a harmful air pollutant that adversely affects both human health and the environment. Short-term exposure to high level of NO₂ can irritate the respiratory system which may exacerbate the symptoms of respiratory diseases such as asthma, while prolonged exposure has been linked to the development of such lung conditions as well as cardiovascular diseases. NO₂ interacting with water, oxygen, and other chemicals can cause damage to the environment in a number of different ways, such as acid rain, smog, and the formation of ozone. Studying the effects of policy interventions and regulation changes that directly or indirectly lead to the reduction of NO₂ emission thus is an important area of research. One example of such indirect policy intervention is the lockdown measures taken across the world. The main source of NO₂ in urban areas such as London is emission from vehicles. A number of studies have shown that restricted mobility due to the lockdown has contributed to a drop in NO₂ concentration in the air on a global scale (See Dutta et al. (2021) and Cooper

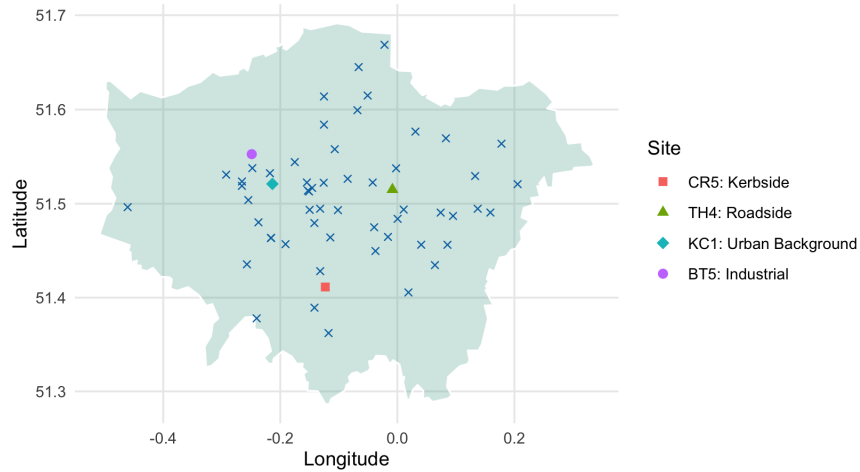


Figure 9: The location of NO₂ measurement sites included in the dataset. Four sites are selected and labelled for illustration purposes. Site CR5 is in the Borough of Croydon, while TH4, KC1 and BT5 are in Tower Hamlets, Kensington and Chelsea, and Brent. The sites in the dataset are classified into 5 categories: Kerbside, Roadside, Urban Background, Suburban and Industrial.

et al. (2022) for example). By examining measurement data from monitoring stations across the country, a comparable conclusion was drawn at the national level in the UK (Higham et al., 2021; Jephcote et al., 2021; J. D. Lee et al., 2020). The majority of such studies analyse the average daily concentrations. While daily mean data are suitable when the research question revolves around assessing long-term changes in the concentration level, interesting findings may be reached by analysing hourly-recorded data. It is known that the concentration of NO₂ in the air varies over the course of a day, with a distinct daily cycle. If we are to investigate the effect of lockdown, in addition to studying the average downtrend, which is typically done by analysing daily or weekly average data, one may ask if the daily cycle changed over time during this period. With measurement data from multiple sites, it is also possible to study spatial patterns, and with that pattern identified, we can conduct further research on spatio-temporal interaction. That is, we can let the daily cycle or global time trend be different at different locations. Answering these questions requires analysis of hourly-measured data over a number of days at different locations, which easily results in massive data. However such data typically have a balanced panel structure as described in the next section, and can be analysed efficiently using the proposed Kronecker approach. In what follows, we demonstrate that the Kronecker method can easily handle large-scale data that are common in spatial and spatio-temporal analysis. Although our data analysis is exploratory, we aim to show that flexible additive Gaussian process models combined with this Kronecker method make it possible to investigate important research questions that would have been otherwise infeasible.

4.1 Dataset

The dataset used in our analysis comprises NO₂ concentration (expressed in $\mu\text{g}/\text{m}^3$) recorded at different sites in the London Air Quality network (<https://www.londonair.org.uk>), during the period between the 6th of January 2020 and the 30th of May, 2020. Out of all available sites in the network, we excluded the sites that recorded more than 30 % missing values or more than 48 consecutive missing values, which resulted

in the total of 59 sites in the dataset (see Figure 9). This gives three level structure as seen in Figure 2, resulting in a sample size of $n = 208,152$. At the top level, we have the location of each site, recorded as Easting and Northing. At the middle and bottom levels, we use the day and the hour of the day as predictors. As discussed in the previous section, using the Kronecker method usually requires a complete grid structure, hence we imputed the remaining missing values according to the steps described in Appendix C.1. Although the method used is rather simple, due to a very small proportion (0.62%) of missing values in the data, we believe that the bias introduced does not have a significant impact. Another issue to consider is the transformation of the response, NO2 concentrations. While they are typically modelled in log-scale in order to remove the right skewness commonly present in air pollutant concentration data, we decided to leave the response variable in the original scale due to the existence of zero and negative records in the data. The negative values are the results of the measurement equipment uncertainty taken into account. The transition from winter time (GMT) to summer time (BST) that fell into the study period was also adjusted (see Appendix C.1).

4.2 Model formulation

As shown in Figure 2, the dataset has a three-dimensional grid structure, with location, day and hour as predictors, denoted by $\mathbf{x}_1 \in \mathcal{X}_1$, $x_2 \in \mathcal{X}_2$ and $x_3 \in \mathcal{X}_3$ where $\mathcal{X}_1 \subset \mathbb{R}^2$, \mathcal{X}_2 represents the set of calendar dates numbered $1, 2, \dots$, and \mathcal{X}_3 represent hour of the day indexed by $1, 2, \dots, 24$. Let $y_{s,d,h}$ denote the observed NO2 concentration from monitoring station s , on day d at hour h where $s = 1, \dots, n_1$, $d = 1, \dots, n_2$, $h = 1, \dots, n_3$ and $n_1 = 59$, $n_2 = 147$, $n_3 = 24$. To model the response, we consider a function of three variables $f : \mathcal{X} = \mathcal{X}_1 \times \mathcal{X}_2 \times \mathcal{X}_3 \rightarrow \mathbb{R}$ and assume a zero mean GP prior. Revising the model in 2.1, we have

$$y_{s,d,h} = f(\mathbf{x}_{1s}, x_{2d}, x_{3h}) + \epsilon_{s,d,h}$$

with $f \sim \text{GP}(0, k)$ where a covariance kernel $k : \mathcal{X} \times \mathcal{X} \rightarrow \mathbb{R}$ is modelled according to our prior belief. We assume i.i.d error with $\epsilon_{s,d,h} \sim N(0, \sigma^2)$. We consider several kernels that belong to a class of hierarchical ANOVA decomposition kernels. Note that for $l = 1, 2, 3$, we denote the base kernel for each predictor by k_l defined on $\mathcal{X}_l \times \mathcal{X}_l$ and assume $f_l \sim \text{GP}(0, k_l)$. The interaction terms are constructed using the tensor product kernel (2.9). For the model specification, we drop the subscripts s, d, h to simplify the expression.

4.2.1 List of models

Model 1: main effect

The first model we consider is the main effect model, where $f(\mathbf{x}_1, x_2, x_3)$ and the kernel are given by

$$\begin{aligned} f(\mathbf{x}_1, x_2, x_3) &= a + f_1(\mathbf{x}_1) + f_2(x_2) + f_3(x_3) \\ k_{m1} &= 1 + k_1 + k_2 + k_3. \end{aligned}$$

The Gram matrix with this kernel and all other kernels under consideration are given in C.2. This model does not involve any interaction effects, meaning that the effect of the location is constant throughout the whole period. Or equivalently, the global time trend captured using the day predictor x_2 and the daily cyclical effect captured by the hour predictor x_3 are both assumed the same for all sites. We use Model 1 as the baseline model and extend it to include two-way or three-way interaction effects.

Model 2: space-time interaction

If we assume a space and time interaction, i.e., the global time trend and daily cycle are different at different location, we have Model 2 specified by

$$\begin{aligned} f(\mathbf{x}_1, x_2, x_3) &= a + f_1(\mathbf{x}_1) + f_2(x_2) + f_3(x_3) + f_{12}(\mathbf{x}_1, x_2) + f_{13}(\mathbf{x}_1, x_2) \\ k_{m2} &= k_{m1} + k_1 \otimes k_2 + k_1 \otimes k_3 \end{aligned}$$

Model 3: all two-way interaction

The model with all two-way interactions extends Model 2 by

$$\begin{aligned} f(\mathbf{x}_1, x_2, x_3) &= a + f_1(\mathbf{x}_1) + f_2(x_2) + f_3(x_3) + f_{12}(\mathbf{x}_1, x_2) + f_{13}(\mathbf{x}_1, x_2) + f_{23}(x_2, x_3) \\ k_{m3} &= k_{m2} + k_2 \otimes k_3 \end{aligned}$$

and adds further assumption that the daily cycle changes over time.

Model 4: saturated/three-way interaction model

If we consider the saturated model with a three-way interaction, the model equals

$$\begin{aligned} f(\mathbf{x}_1, x_2, x_3) &= a + f_1(\mathbf{x}_1) + f_2(x_2) + f_3(x_3) + \\ &\quad f_{12}(\mathbf{x}_1, x_2) + f_{13}(\mathbf{x}_1, x_2) + f_{23}(x_2, x_3) + f_{123}(\mathbf{x}_1, x_2, x_3) \\ k_{m4} &= k_{m3} + k_1 \otimes k_2 \otimes k_3 \end{aligned}$$

Note that this is the saturated ANOVA decomposition kernel for data with a three-dimensional grid structure.

Model 5: three-way interaction only

Finally, we also fit a model with only the three-way interaction term, of which the model function f and the kernel are given by

$$\begin{aligned} f(\mathbf{x}_1, x_2, x_3) &= f_{123}(\mathbf{x}_1, x_2, x_3) \\ k_{m5} &= k_1 \otimes k_2 \otimes k_3. \end{aligned}$$

Although this separable kernel is widely used in machine learning applications, with this kernel construction, the interpretation of the effects of each predictor is difficult. The result shows that it fits the data poorly compared to other models under consideration.

4.2.2 Considerations for data structure

Another way to approach the problem is treating the data as a two-dimensional structure with location and time represented in hours from 0 to $24 \times 147 = 3528$, as predictors and using a combination of multiple kernels to model the temporal structure. For example, it is common to use one or more kernels to model the global trend (e.g. squared exponential (2.5) or Matérn (A.1)), and another kernel to model the cyclical effect (e.g. squared exponential periodic kernel (A.2)). With this model formulation, it may be difficult to separate the cyclical effect and short-term variations in the global time trend. This may result in the estimate of the length-scale parameter ρ in the kernel for the global time trend being too short. Our approach with a three-level structure avoids this by more directly modelling the two effects using the hour of the day and

Model	α_0	α_1	α_2	α_3	σ	$\Delta\text{mloglik}$	Time
1: main	5.4278	16.1830	11.1906	2.0739	14.8513	-	13.3
2: spatio-temporal interaction	5.3596	5.9054	3.9376	0.8802	12.4446	23,652	19.4
3: all two-way interaction	5.4239	6.9452	4.6886	0.9336	8.3439	96,739	16.9
4: saturated	5.4323	3.2828	5.0512	0.1650	6.5033	81,567	17.9
5: three-way interaction only	-	0.0008052	-	-	36.4303	-186,450	1.96

Table 1: Results from fitting Model 1 to Model 5 to London NO₂ data. We use the posterior means as point estimates for each hyper-parameter and evaluate the log marginal likelihood using the estimates. The difference of the log marginal likelihood in comparison to that of the baseline model (Model 1) is shown as $\Delta\text{mloglik}$. The log marginal likelihood for Model 1 is -858000. The average time (in minutes) taken to obtain 2 chains of 300 MCMC samples after the 200 warm-up phase is also displayed. For model 5, we only need one scale parameter α_1 due to identifiability issues.

calendar day. The three-level approach also has a computational advantage; instead of working on a matrix of size 3528×3528 , we only have to handle 24×24 and 147×147 matrices.

4.2.3 Kernel choice

The choice of baseline kernels k_l is also an important factor that reflects our prior belief about the underlying process. As discussed in Section 2.3, a GP with the squared-centred standard Brownian motion kernel ($\gamma = 0.5$) has good smoothness properties. This kernel, as well as other fractional Brownian motion-based kernels, has a computational advantage over other common kernels such as squared exponential kernels, as we do not have to perform eigen-decomposition or matrix-vector multiplication at each iteration of a chosen optimisation algorithm. We use this as a starting point and explore different options. We found that the spatial process f_1 is rougher than the temporal processes f_2, f_3 . To determine the optimal values for the Hurst coefficient γ in k_1 , we conducted a grid search, which led to the choice of $\gamma = 0.3$. For k_2 and k_3 , squared-centred standard Brownian motion kernels ($\gamma = 0.5$) produced a good fit. We put priors on the rest of the hyper-parameters, including the scale parameters of the kernels $\alpha_1, \alpha_2, \alpha_3$, and the variance of the error term σ^2 and estimated them by the posterior mean from MCMC samples. The specified models are implemented using the programming language Stan.

4.3 Results

The main results are shown in Table 1, including the point estimates of hyper-parameters, log marginal likelihood improvement compared to the baseline model and computational time. From the log marginal likelihood values, we see a potential over-fit of the saturated model, and that the all two-way interaction model (Model 3) is the best model. Except for Model 5, the MCMC sampling took less than 20 minutes on average, which is reasonable for this size of the data. Note that Model 5 only has two model parameters. It can also be seen that the interaction-only model performs worse than the simple main effect model. In Figure 10, we show the posterior mean and the 2.5% and 97.5% quantiles of the posterior predictive distribution derived by Model 3, at selected sites (see Table 9) from the 23rd of March for two weeks together with the corresponding observed values. We can see that the posterior predictive mean captures the overall trend well, but smoother than the observed.

The model comparison implies that, on top of the space-time interaction, the effect of the hours of the day interacts with the effects of global time. That is, the global time trend and the daily cycle of NO₂ concentration level are different for different locations, and the identified daily cycle also changes over time.

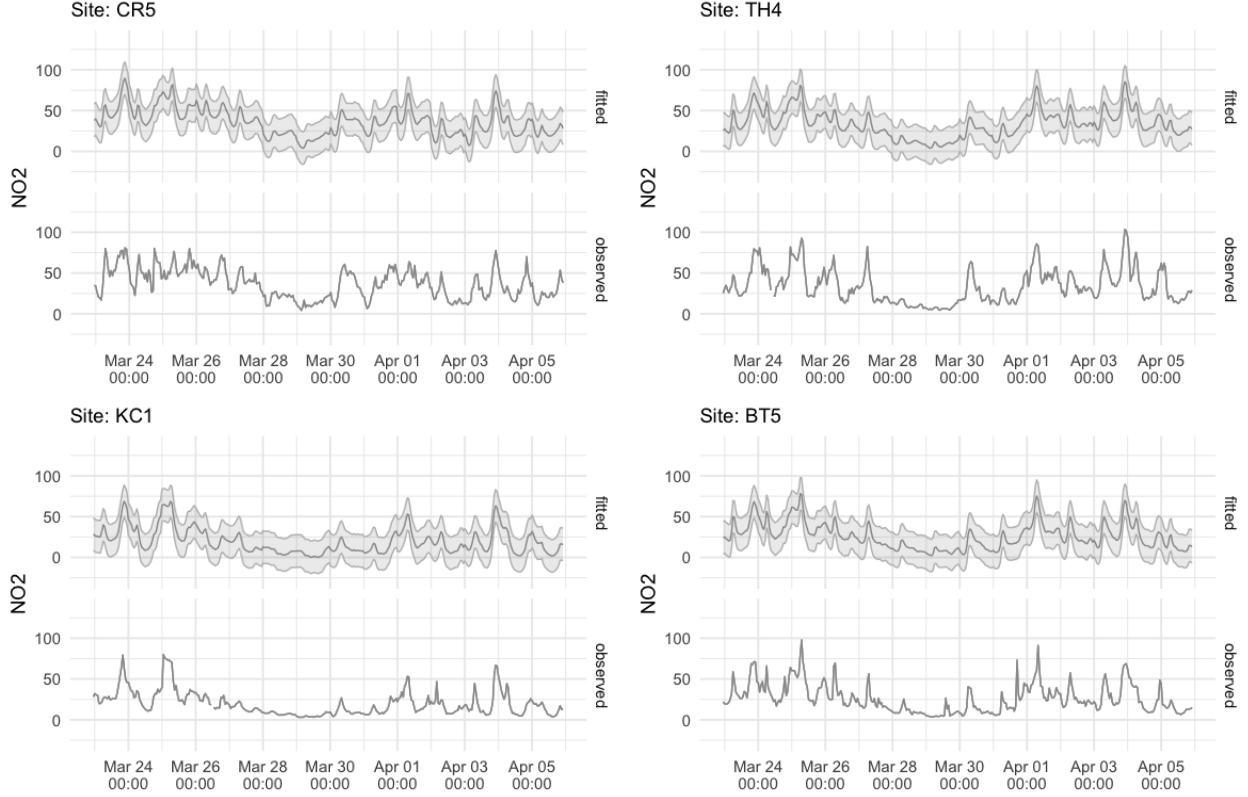


Figure 10: Observed and fitted (with 95% predictive bands) NO2 concentrations at 4 different site

However, the fact that the additional three-way interaction term did not lead to improvement in log marginal likelihood suggests that this change in daily pattern over time is the same for all measurement sites. To demonstrate this, we can visualise each effect by using the mean and variance decomposition of additive GP models seen in (2.22) and (2.23). Figure 11 shows the estimated daily cycle at the selected sites. It is noticeable that Station CR5 and Station TH4 which are located in Kerbside and Roadside respectively, have two peaks in the morning and in the evening, corresponding to rush hours. The station in the background, KC1, also shows two peaks, however, the magnitude of the effect is much smaller compared to CR5 and TH4. Station BT5 is close to an industrial site and with only one peak in the morning. From the figure, we see a clear interaction effect between the hour of the day and the location of the site. Another way to look at the interaction effect is to investigate how the spatial variation changes over time (see Figure 12). Figure 13 shows the interaction effect between the global time and the hour of the day for selected weeks. During the week commencing on the 27th of January (week 5 of 2020), there are two clear peaks in the beginning of the week, but this pattern becomes less clear over the course of the week. During the weekend, the magnitude of the effect becomes smaller. The week starting on the 23rd of March (week 14), where the first COVID-19 lockdown in the UK took place, shows more irregular patterns. The Monday of this week is the day that the British Prime Minister announced the plan to introduce the measure which legally came into force 3 days later. The first national lockdown lasted the next few months with parts of the restriction being lifted from mid-May. The last two plots show the effect in the week starting on the 20th of April (week 17) and on the 25th of May (week 22). There is a distinct peak in the morning for many of the days, but the evening peak is much less apparent compared with week 5. The interaction effect between global time (day) and location

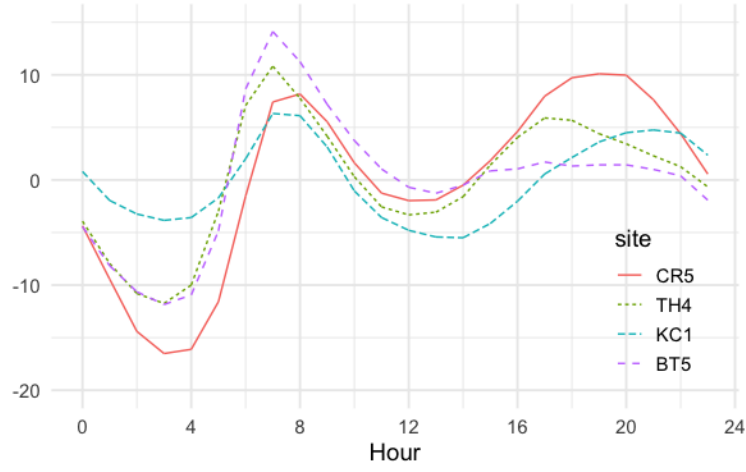


Figure 11: Hour of the day effect on NO₂ in $\mu\text{g}/\text{m}^3$ by site

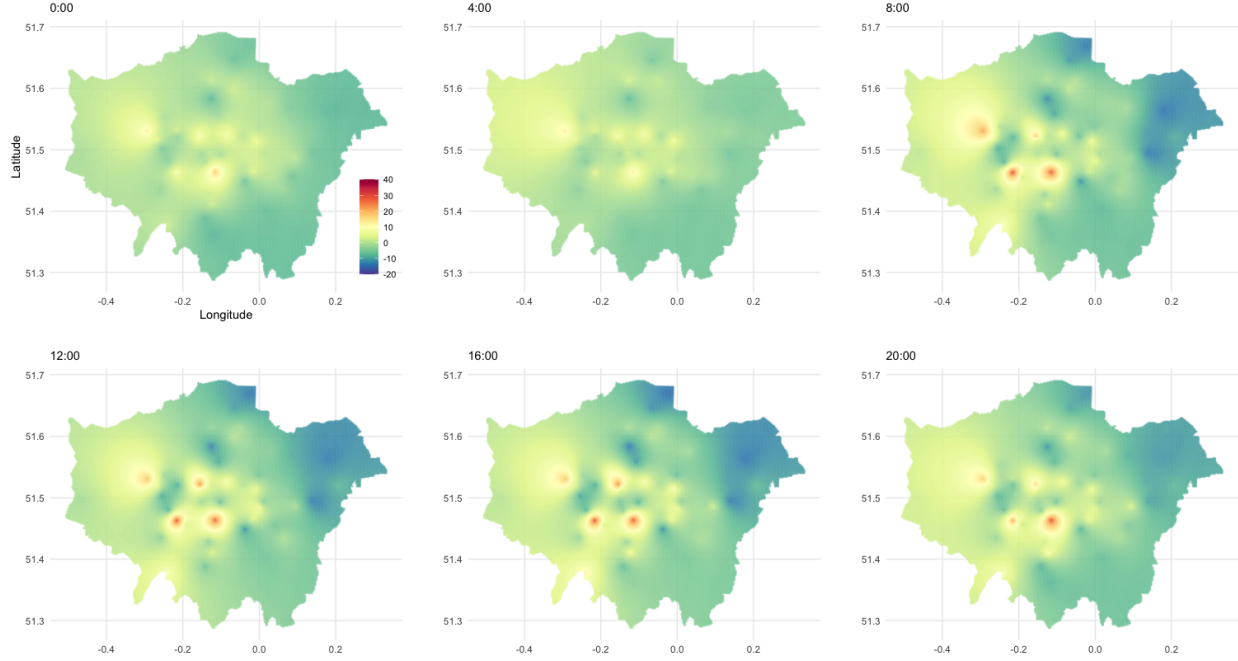


Figure 12: The spatial effect over London at different hours of the day with the calendar date held constant. The effect is measured in $\mu\text{g}/\text{m}^3$

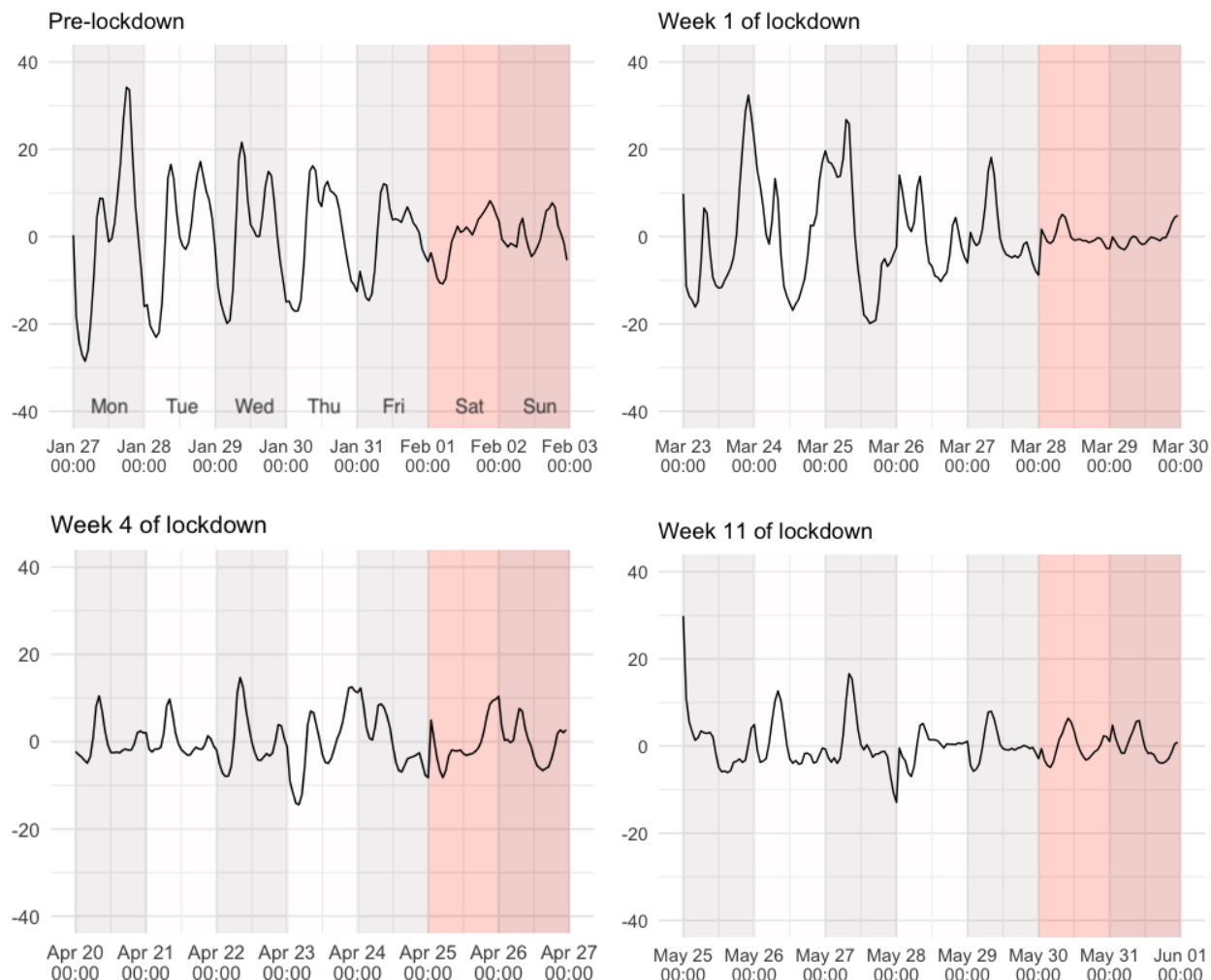


Figure 13: The interaction effect between global time (day) and hour of the day.

can be visualised by plotting the effect of global time by sites (see Figure 14). Except for CR5, we see a small downward trend over the period. Whether this is the effect of the lockdown or the result of lower emission from e.g. heating source due to warmer weather needs further investigation. For example, we can compare the records from previous years, or incorporate information such as temperature in the model. Short-term variation is also apparent in all panels in Figure 14. There are many factors to consider in explaining this variation. One possibility is the weekend effect associated with less traffic. Looking at the panels in the figure, we see that some troughs in the figure seem to fall into weekend although there are some deviations from this pattern. This may be due to some meteorological factors affecting the concentration level of the pollutant. For example, it is well-known that lower wind speeds are associated with higher concentrations. The two-week period starting on the 12th of January sees one large peak across the sites, which corresponds with the trough in the wind speed. Other weather conditions such as temperature, precipitation or sunlight also affect the levels of NO_2 concentrations in the air. Including meteorological data as covariates can help improve the fit, as well as estimate and visualise the time trend after removing the effect of the weather conditions. If the weekly pattern is still apparent, we can introduce another level in the data structure, i.e., a four-dimensional grid structure, and gain further computational efficiency.

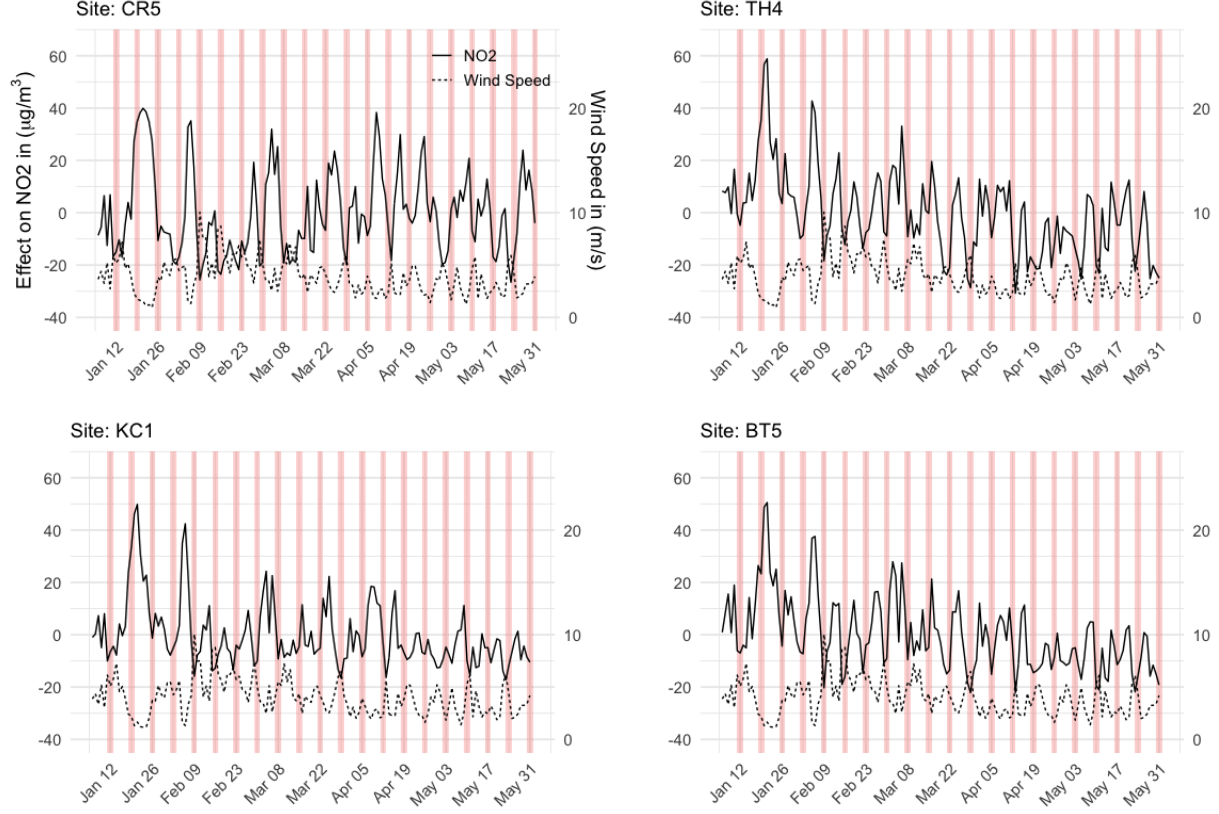


Figure 14: The global time (day) effect and wind speed by site with weekends highlighted. Low wind speed corresponds to a higher level of pollution

5 Discussion

This paper proposed a class of Additive GP models using saturated and hierarchical ANOVA decomposition kernels. This is a natural way of constructing additive models that allow for modelling main effects and interaction effects without increasing the number of model parameters and offers a straightforward interpretation of the fitted model. Furthermore, we showed that with kernels being centred, the popular Kronecker product approach can be extended to handle various structures of interaction effect models. This allows for the analysis of large-scale multidimensional grid data without assuming a saturated model.

The proposed method is applied to efficiently analyze hourly-recorded ambient NO₂ concentrations in London for the period covering both before and after the COVID-19 lockdown measure was introduced. We treated the data as three-dimensional grid data, with the location of the monitoring stations, day, and hour of the day as three predictors. The effect of three variables can be seen as the spatial effect, global time effect and daily cyclic effect respectively. We considered five regression models of the three variables, including the main effect model, two kinds of two-way (hierarchical) interaction models, the three-way (hierarchical) interaction (saturated) model, and the three-way interaction only model. We compared the models in terms of the marginal likelihood and found that the all two-way interaction model, and not the saturated model, is the best fit for the data, suggesting that the global time trend and the daily cycle are different for different locations, with the latter changing over time. An efficient implementation of this model had not been possible under the existing Kronecker approach. It is also important to note that the success of our approach does not

reduce the significance of other scalable approaches to GP regression that can be used for more general data structures such as a subset of data, Nyström approximation, inducing points methods, sparse variational methods, or vice versa. In fact, the Kronecker approach, including our proposal, can be combined with such methods, which can then facilitate the analysis of even larger datasets than the one considered in this paper.

We would like to point out that, while it is not considered in our data analysis, the inclusion of other covariates such as information related to monitoring stations, or meteorological variables is possible under the proposed model. If the covariates are level specific, e.g. types of the monitoring stations (roadside, background etc.) at the top level, or daylight time in London at the middle level, we can simply add the centred covariance function for each covariate to the kernel given at each level, which in this example, are the kernels for location and day, respectively. However, many meteorological variables are observed at the cross-level. For example, we may want to use hourly-recorded wind speed or precipitation at different locations. If the effect of these meteorological variables is linear (including polynomial), we can incorporate them into a model while still avoiding cubic time complexity, by combining the idea of modelling explicit basis functions (Rasmussen & Williams, 2006, Chapter 2.7) with our Kronecker approach. Using such information in the model is especially important if prediction is the main interest. In this case, we should consider additional model assessment criteria to marginal likelihood, that is more targeted at predictive accuracy, such as mean squared error or log loss for test data.

Another issue worth exploring is the problem of missing values. Our method can handle data with a complete grid structure, i.e., no missing values. This may not always be a reasonable assumption for real-world applications. For example, in air quality monitoring, the monitoring device can malfunction for several hours to several days. Repeated measurements in social, psychological, or medical science commonly suffer from dropout. In this paper, we excluded some monitoring sites that have many missing records and imputed the rest of the missing values by a simple procedure. If the proportion of missing values in the data is large, more sophisticated approaches should be considered to avoid potential bias. Gilboa et al. (2013) and Wilson et al. (2014) proposed an approximation to the likelihood in the presence of missing values in multidimensional grid structure data. Our future work will focus on this issue. In particular, the proposed method can be incorporated into an algorithm that sequentially imputes missing values and estimates model parameters.

A Kernel, Gaussian process and Reproducing Kernel Hilbert Space

A.1 Different kernels

Common kernels

The examples below are some of the most commonly used kernels. Note that as in SE kernel (2.5) all kernel have a scale parameter $\alpha > 0$ and some also share another parameter $\rho > 0$, called length-scale. Let $\mathbf{x}, \mathbf{x}' \in \mathbb{R}^m$ and $t, t' \in \mathbb{R}$ and $c > 0$ be a constant.

1. Matérn class kernel (Matérn (1960), Stein (1999)):

$$k_{mat}(\mathbf{x}, \mathbf{x}') = \alpha^2 \frac{2^{1-\nu}}{\Gamma(\nu)} \left(\frac{\sqrt{2\nu} \|\mathbf{x} - \mathbf{x}'\|}{\rho} \right)^\nu K_\nu \left(\frac{\sqrt{2\nu} \|\mathbf{x} - \mathbf{x}'\|}{\rho} \right), \quad (\text{A.1})$$

where K_ν is a modified Bessel function. The parameter $\nu > 0$ determines the roughness of the

corresponding process.

2. Periodic kernel:

$$k_{pr}(t, t') = \alpha^2 \exp \left(-\frac{2 \sin^2 \left(\frac{\pi |t-t'|}{p} \right)}{\rho^2} \right), \quad (\text{A.2})$$

where $p > 0$, period parameter, can be treated as known or unknown. Corresponding GP is a periodic function of period p .

3. Polynomial kernel

$$k_{pol}(\mathbf{x}, \mathbf{x}') = \alpha^2 (\mathbf{x}^\top \mathbf{x}' + c)^d, \quad (\text{A.3})$$

where $m \in \mathbb{N}$. With $d = 1$ we have linear kernel.

4. Constant kernel

$$k_{const}(\mathbf{x}, \mathbf{x}') = c \quad (\text{A.4})$$

With Matérn class kernels, the smoothness of the process can be controlled by parameter ν . With $\nu = 1.5$ process is rough (see figure 15) compared with $\nu = 2.5$. It is worth noting that for $\nu \rightarrow \infty$, eq.A.1 equals S.E. kernel. Periodic kernel is useful when handling the continuous-time process that has a regular cycle, e.g. daily, weekly or annually. It can be derived from S.E. kernel; we have $k_{se}(\mathbf{u}, \mathbf{u}') = k_{pr}(t, t')$ where $\mathbf{u} = (\sin(\frac{p}{2\pi}t), \cos(\frac{p}{2\pi}t))^\top$. In fact any kernel k can be made periodic with this formulation. The constant kernel is usually used in combination with other kernels, such as our example in (2.10).

Stationary and non-stationary kernel

SE kernel, Matérn kernel, and periodic kernel constructed from SE kernel are in the class of stationary kernel, more specifically isotropic kernel. A stationary kernel is a function of a lag vector $\tau = \mathbf{x} - \mathbf{x}'$ of two inputs. When the value of the function depends only on the norm of the two inputs $r = \|\tau\|$, the kernel is said to be isotropic and the corresponding process is invariant under shift in time or space. While the assumption of isotropy or stationarity gives a nice interpretation of correlation structure, we need a class of non-stationary kernels in the case where this assumption does not hold. A few simple examples of non-stationary kernels include linear kernel and polynomial kernel. Using these kernels in Gaussian process regression corresponds with Bayesian linear or polynomial regression. Another useful non-stationary kernel is the fractional Brownian Motion kernel 2.15 and kernels that are constructed from this kernel, such as its centred version.

A.2 Kernel sums and products

Given valid kernels k_1 and k_2 on \mathcal{X} , a function $k : \mathcal{X} \times \mathcal{X} \rightarrow \mathbb{R}$ constructed as their sum or product

$$\begin{aligned} k(\mathbf{x}, \mathbf{x}') &= k_1(\mathbf{x}, \mathbf{x}') + k_2(\mathbf{x}, \mathbf{x}') \\ k(\mathbf{x}, \mathbf{x}') &= k_1(\mathbf{x}, \mathbf{x}') k_2(\mathbf{x}, \mathbf{x}') \end{aligned}$$

constitutes a positive definite kernel. The kernel k_1 or k_2 can be a (positive) constant kernel (A.4). Hence, adding a positive constant or multiplying by a positive constant gives a positive definite kernel. It is also important to note that it is not necessary that k_1 and k_2 are defined on the same set. For example, given

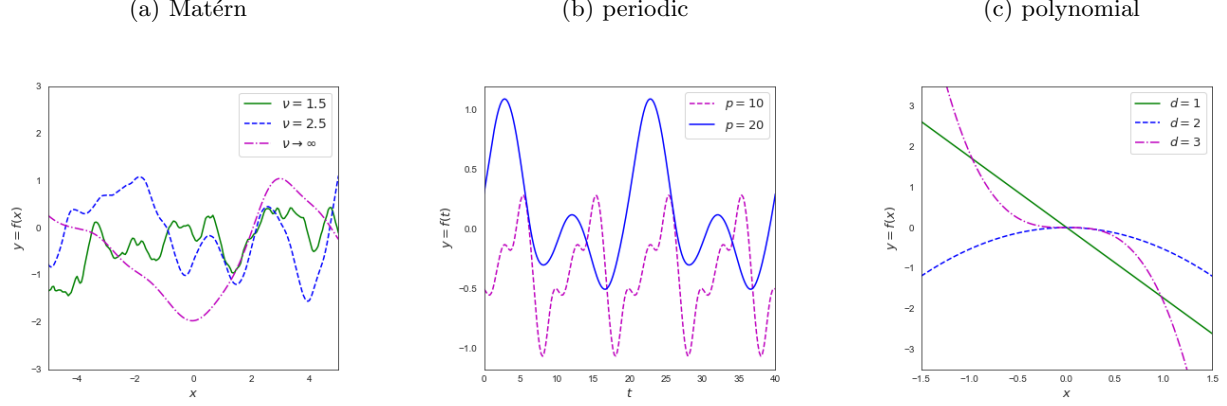


Figure 15: Sample paths from zero mean Gaussian process with different kernels. For all panels, the scale parameter α is set to be 1, and the length-scale parameter $\rho = 1$ for (a) and (b). For polynomial kernel, $c = 0$. For the additional parameters see the legend of each panel.

$k_1 : \mathcal{X} \times \mathcal{X} \rightarrow \mathbb{R}$ and $k_2 : \mathcal{S} \times \mathcal{S} \rightarrow \mathbb{R}$, then $k : \mathcal{D} \times \mathcal{D} \rightarrow \mathbb{R}$ where $\mathcal{D} = \mathcal{X} \times \mathcal{S}$ given by

$$k((\mathbf{x}, \mathbf{s}), (\mathbf{x}', \mathbf{s}')) = 1 + k_1(\mathbf{x}, \mathbf{x}') + k_2(\mathbf{s}, \mathbf{s}') + k_1(\mathbf{x}, \mathbf{x}')k_2(\mathbf{s}, \mathbf{s}')$$

is a positive definite kernel.

A.3 Posterior in GPR

Let us consider the regression model considered in Section 2.4, i.e., we have

$$\mathbf{y} = (y_1, \dots, y_n)^\top \sim \text{MVN}_n(\mathbf{0}, \mathbf{K} + \sigma^2 \mathbf{I}). \quad (\text{A.5})$$

Let us assume that we have $\mathbf{x}_j^* \in \mathcal{X}$ for $j = 1, \dots, m$ with $\mathbf{x}_j^* \in \mathcal{X}$. This set of \mathbf{x}_j^* can include \mathbf{x}_i in a sample (training set). We denote $\mathbf{f}^* = (f(\mathbf{x}_1^*), \dots, f(\mathbf{x}_m^*))$. From our prior we know

$$\mathbf{f}^* \sim \text{MVN}_m(\mathbf{0}, \mathbf{K}_{**}) \quad (\text{A.6})$$

where $\mathbf{K}_{**} = \{k_{i,j}^{**}\}_{m \times m}$ and $k_{i,j}^{**} = k(\mathbf{x}_i^*, \mathbf{x}_j^*)$. Hence we have

$$\begin{bmatrix} \mathbf{y} \\ \mathbf{f}^* \end{bmatrix} \sim \text{MVN}_{n+m} \left(\begin{bmatrix} \mathbf{0} \\ \mathbf{0} \end{bmatrix}, \begin{bmatrix} \mathbf{K} + \sigma^2 \mathbf{I} & \mathbf{K}_* \\ \mathbf{K}_*^\top & \mathbf{K}_{**} \end{bmatrix} \right). \quad (\text{A.7})$$

where $\mathbf{K}_* = \{k_{i,j}^*\}_{n \times m}$ and $k_{i,j}^* = k(\mathbf{x}_i, \mathbf{x}_j^*)$. By conditional distribution of multivariate normal distribution,

$$\mathbf{f}^* | \mathbf{X}, \mathbf{X}^*, \mathbf{y} \sim \text{MVN}_m(\boldsymbol{\mu}^*, \mathbf{V}^*) \quad (\text{A.8})$$

where

$$\boldsymbol{\mu}^* = \mathbf{K}^{*\top}(\mathbf{K} + \sigma^2 \mathbf{I})^{-1} \mathbf{y} \quad (\text{A.9})$$

$$\mathbf{V}^* = \mathbf{K}_{**} - \mathbf{K}^{*\top}(\mathbf{K} + \sigma^2 \mathbf{I})^{-1} \mathbf{K}_*. \quad (\text{A.10})$$

It is easy to see that we have $\boldsymbol{\mu}^* = (\bar{m}(\mathbf{x}_1^*), \dots, \bar{m}(\mathbf{x}_1^*))$ and $\mathbf{V}^* = \{v_{i,j}^*\}_{m \times m}$ with $v_{i,j}^* = \bar{k}(\mathbf{x}_i^*, \mathbf{x}_j^*)$ where $\bar{m} : \mathcal{X} \rightarrow \mathbb{R}$ and $\bar{k} : \mathcal{X} \times \mathcal{X} \rightarrow \mathbb{R}$ are given by

$$\begin{aligned}\bar{m}(\mathbf{x}) &= \mathbf{k}(\mathbf{x})^\top (\mathbf{K} + \sigma^2 \mathbf{I})^{-1} \mathbf{y}, & \mathbf{x} &\in \mathcal{X} \\ \bar{k}(\mathbf{x}, \mathbf{x}') &= k(\mathbf{x}, \mathbf{x}') - \mathbf{k}(\mathbf{x})^\top (\mathbf{K} + \sigma^2 \mathbf{I})^{-1} \mathbf{k}(\mathbf{x}'), & \mathbf{x}, \mathbf{x}' &\in \mathcal{X}.\end{aligned}$$

By Kolmogorov extension theorem and Definition 2, this implies that the posterior is the Gaussian process $GP(\bar{m}, \bar{k})$.

A.4 Reproducing kernel Hilbert space

Recall that Hilbert space is a complete inner product space equipped with a positive definite inner product. Let \mathcal{H} be a Hilbert space of functions over a set \mathcal{X} with an inner product $\langle \cdot, \cdot \rangle_{\mathcal{H}}$. The Hilbert space \mathcal{H} is called a reproducing kernel Hilbert space (RKHS) if and only if there exists a function $k : \mathcal{X} \times \mathcal{X} \rightarrow \mathbb{R}$ satisfying

1. $k(x, \cdot) \in \mathcal{H}$ for all $x \in \mathcal{X}$
2. $f(x) = \langle f, k(x, \cdot) \rangle_{\mathcal{H}}$ for all $f \in \mathcal{H}$ and $x \in \mathcal{X}$

The function k is called reproducing kernel. Note that using the two properties, we have that $k(x, x') = \langle k(x, \cdot), k(x', \cdot) \rangle_{\mathcal{H}}$, hence k is positive definite. It can be shown by the Moore–Aronszajn theorem (Aronszajn (1950)) that a kernel defines a unique RKHS and vice versa. We write the norm of a function f in \mathcal{H} as $\|f\|_{\mathcal{H}} = \sqrt{\langle f, f \rangle}$.

A.5 centring of kernel and functions in RKHS

Let P be distribution over \mathcal{X} and $X, X' \in \mathcal{X}$ are independent and follow P . We consider a kernel k on \mathcal{X} and let \mathcal{H}_k denote the RKHS induced by k . We can center this kernel by,

$$k_{cent}(x, x') = \langle k(x, \cdot) - \mu_P, k(x', \cdot) - \mu_P \rangle_{\mathcal{H}_k} \quad (\text{A.11})$$

where μ_P is the kernel mean given by

$$\mu_P := \mathbb{E}_{X \sim P} [k(X, \cdot)] = \int_{\mathcal{X}} k(x, \cdot) dP(x). \quad (\text{A.12})$$

Note that the expectation of any function $f \in \mathcal{H}_k$ can be computed as an inner product with μ_P :

$$\begin{aligned}\mathbb{E}_{X \sim P} [f(X)] &= \int_{\mathcal{X}} f(x) dP(x) \\ &= \int_{\mathcal{X}} \langle k(x, \cdot), f \rangle_{\mathcal{H}_k} dP(x) \\ &= \langle \int_{\mathcal{X}} k(x, \cdot) dP(x), f \rangle_{\mathcal{H}_k} = \langle \mu_P, f \rangle_{\mathcal{H}_k}.\end{aligned} \quad (\text{A.13})$$

The centred kernel is positive definite by construction. We can see that this corresponds with (2.13) by

$$\begin{aligned}\langle k(x, \cdot) - \mu_P, k(x', \cdot) - \mu_P \rangle_{\mathcal{H}_k} &= \langle k(x, \cdot), k(x', \cdot) \rangle_{\mathcal{H}_k} - \langle \mu_P, k(x', \cdot) \rangle_{\mathcal{H}_k} - \langle k(x, \cdot), \mu_P \rangle_{\mathcal{H}_k} + \langle \mu_P, \mu_P \rangle_{\mathcal{H}_k} \\ &= k(x, x') - \mathbb{E}_{X \sim P} [k(x', X)] - \mathbb{E}_{X' \sim P} [k(X', x)] + \mathbb{E}_{X, X' \sim P} [k(X, X')].\end{aligned}\quad (\text{A.14})$$

Note that

$$\begin{aligned}\mathbb{E}_{X, X' \sim P} [k(X, X')] &= \int_{\mathcal{X}} \int_{\mathcal{X}} k(x, x') dP(x) dP(x') \\ &= \int_{\mathcal{X}} \int_{\mathcal{X}} \langle k(x, \cdot), k(x', \cdot) \rangle_{\mathcal{H}_k} dP(x) dP(x') \\ &= \langle \int_{\mathcal{X}} k(x, \cdot) dP(x), \int_{\mathcal{X}} k(x', \cdot) dP(x') \rangle_{\mathcal{H}_k} = \langle \mu_P, \mu_P \rangle_{\mathcal{H}_k}.\end{aligned}\quad (\text{A.15})$$

Given a sample x_1, \dots, x_n drawn from P , the kernel mean μ_P can be estimated empirically, by

$$\hat{\mu}_P = \frac{1}{n} \sum_{i=1}^n k(x_i, \cdot). \quad (\text{A.16})$$

By replacing μ_P with $\hat{\mu}_P$, we get (2.14).

A.6 Eigen-decomposition of a centred Gram matrix

Consider a $n \times n$ Gram \mathbf{K}^c matrix given by a centred kernel function (2.14). In what follows we show that a centred Gram matrix has an eigen-decomposition of a special form. We write an eigen-decomposition of a matrix \mathbf{M} by

$$\mathbf{M} = \mathbf{Q} \mathbf{\Lambda} \mathbf{Q}^\top \quad (\text{A.17})$$

where $\mathbf{\Lambda}$ is a diagonal matrix of which diagonal element are eigenvalues of \mathbf{M} in non-decreasing order and \mathbf{Q} is an orthonormal matrix with its i -th column \mathbf{q}_i given by the eigenvectors which corresponds to i -th eigenvalue. For a centred Gram matrix, we have the following.

Lemma 2. *Any eigenvector \mathbf{q}_i of a centred Gram matrix $\mathbf{K}^{(c)}$ associated with non-zero eigenvalue λ_i is orthogonal to $\mathbf{1}$.*

Proof. Using $\mathbf{K}^{(c)} \mathbf{q}_i = \lambda_i \mathbf{q}_i$, we have

$$\mathbf{q}_i^\top \mathbf{1} = \frac{1}{\lambda_i} \mathbf{q}_i^\top \mathbf{K}^{(c)} \mathbf{1} = 0. \quad (\text{A.18})$$

The last equality is due to the fact that all rows and columns of a centred matrix sums to 0. \square

Lemma 3. *A centred Gram matrix $\mathbf{K}^{(c)}$ has the following eigen-decomposition:*

$$\mathbf{K}^{(c)} = \mathbf{Q}^{(c)} \mathbf{\Lambda}^{(c)} \mathbf{Q}^{(c)\top} \quad (\text{A.19})$$

where

$$\text{diag}(\mathbf{\Lambda}^{(c)}) = (0, \lambda_2, \dots, \lambda_n)^\top, \lambda_j \geq 0 \ \forall j \in \{2, \dots, n\} \quad (\text{A.20})$$

and

$$\mathbf{Q}^{(c)} = \begin{bmatrix} \frac{1}{\sqrt{n}} & & & \\ \vdots & \mathbf{q}_2 & \cdots & \mathbf{q}_n \\ \frac{1}{\sqrt{n}} & & & \end{bmatrix}. \quad (\text{A.21})$$

Proof. Let k denote the number of zero eigenvalues of $\mathbf{K}^{(c)}$. Due to the centring, $\text{rank}(\mathbf{K}^{(c)}) \leq n - 1$, i.e., we have $k \geq 1$.

For $k = 1$, we have $\lambda_j > 0, \forall j \in \{2, \dots, n\}$ and the eigenvectors $\mathbf{q}_2, \dots, \mathbf{q}_n$ are orthogonal to $\mathbf{1}$ from lemma 2. Normalising the vector $\mathbf{1}$ completes an orthonormal basis, hence the first column of $\mathbf{Q}^{(c)}$ is given by $\frac{1}{\sqrt{n}}\mathbf{1}$. For $k \geq 2$, the first k columns of $\mathbf{Q}^{(c)}$, $(\mathbf{q}_1, \dots, \mathbf{q}_k)$, are not uniquely determined. Using $\mathbf{q}_j^\top (\frac{1}{\sqrt{n}}\mathbf{1}) = \frac{1}{\sqrt{n}}\mathbf{q}_j^\top \mathbf{1} = 0$ for $j = k + 1, \dots, n$, we set $\mathbf{q}_1 = \frac{1}{\sqrt{n}}\mathbf{1}$ and find $(\mathbf{q}_2, \dots, \mathbf{q}_k)$ to complete an orthonormal system. \square

In practice, we may use a computer program to obtain a initial set of normalised eigen-vectors denoted by $\mathbf{v}_1, \dots, \mathbf{v}_n$. For $k \geq 2$, $\mathbf{v}_1, \dots, \mathbf{v}_k$ may not contain a vector $\frac{1}{\sqrt{n}}\mathbf{1}$ but $\text{span}(\mathbf{v}_1, \dots, \mathbf{v}_k)$ contains $\mathbf{1}$. To have orthonormal bases $\mathbf{q}_1, \dots, \mathbf{q}_n$ specified above, we take $\mathbf{q}_1 = \frac{1}{\sqrt{n}}\mathbf{1}$ and $\mathbf{q}_j = \mathbf{v}_j$ for $j = k + 1, \dots, n$. The rest of the vectors $\mathbf{q}_2, \dots, \mathbf{q}_k$ can be computed using for example Gram-Schmidt process.

Remark 1. The $n \times n$ matrix $\mathbf{1}\mathbf{1}_n^\top$ has the following decomposition:

$$\mathbf{1}\mathbf{1}_n^\top = \mathbf{Q}^{(c)} \mathbf{A}_n \mathbf{Q}^{(c)\top} \quad (\text{A.22})$$

where $\mathbf{Q}^{(c)}$ is given by (A.21) and \mathbf{A}_n is a $n \times n$ matrix with i, i -th element n and 0 everywhere else, i.e.,

$$\mathbf{A}_n = \begin{bmatrix} n & 0 & \cdots & 0 \\ 0 & 0 & \cdots & 0 \\ \vdots & \vdots & \ddots & \vdots \\ 0 & 0 & \cdots & 0 \end{bmatrix}. \quad (\text{A.23})$$

B Kronecker methods

B.1 Kronecker product and its properties

Kronecker product

Consider two matrices $\mathbf{A} = \{a_{i,j}\}_{1 \leq i \leq n, 1 \leq j \leq m}$ and $\mathbf{B} = \{b_{i,j}\}_{1 \leq i \leq p, 1 \leq j \leq q}$. The Kronecker product of the two matrices, $\mathbf{A} \otimes \mathbf{B}$, is the matrix of size $np \times mq$ given by

$$\mathbf{A} \otimes \mathbf{B} = \begin{bmatrix} a_{1,1}\mathbf{B} & \cdots & a_{1,m}\mathbf{B} \\ \vdots & \ddots & \vdots \\ a_{n,1}\mathbf{B} & \cdots & a_{n,m}\mathbf{B} \end{bmatrix} \quad (\text{B.1})$$

More generally, we denote the Kronecker product of $d \geq 2$ matrices, \mathbf{A}_l where $l = 1, \dots, d$ by

$$\mathbf{A} := \bigotimes_{l=1}^d \mathbf{A}_l \quad (\text{B.2})$$

If each matrix \mathbf{A}_l is size $n_l \times m_l$, the resulting Kronecker product matrix \mathbf{A} has size $\prod_{l=1}^d n_l \times \prod_{l=1}^D m_l$.

Kronecker product properties

We list some of the properties of Kronecker product that we use in this paper. In addition to \mathbf{A}_l defined above, let us assume we have, for $l = 1, \dots, d$, \mathbf{B}_l of size $p_l \times q_l$, \mathbf{B}'_l of size $p_l \times q_l$, \mathbf{C}_l of size $h_l \times k_l$ and \mathbf{D}_l of size $m_l \times p_l$. The size of matrices is given so that the operations $\mathbf{B}_l + \mathbf{B}'_l$ and $\mathbf{A}_l \mathbf{D}_l \mathbf{B}_l$ are allowed.

1. Bilinearity:

$$\mathbf{A}_l \otimes (\mathbf{B}_l + \mathbf{B}'_l) = \mathbf{A}_l \otimes \mathbf{B}_l + \mathbf{A}_l \otimes \mathbf{B}'_l \quad (\text{B.3})$$

2. Associativity:

$$\mathbf{A}_l \otimes (\mathbf{B}_l \otimes \mathbf{C}_l) = (\mathbf{A}_l \otimes \mathbf{B}_l) \otimes \mathbf{C}_l \quad (\text{B.4})$$

$$\alpha(\mathbf{A}_l \otimes \mathbf{B}_l) = (\alpha \mathbf{A}_l) \otimes \mathbf{B}_l = \mathbf{A}_l \otimes (\alpha \mathbf{B}_l) \quad (\text{B.5})$$

where α is a scalar.

3. Transpose:

$$\left(\bigotimes_{l=1}^d \mathbf{A}_l \right)^\top = \bigotimes_{d=l}^d \mathbf{A}_l^\top \quad (\text{B.6})$$

4. Inverse:

$$\left(\bigotimes_{l=1}^d \mathbf{A}_l \right)^{-1} = \bigotimes_{d=l}^d \mathbf{A}_l^{-1} \quad (\text{B.7})$$

5. The mixed product properties:

$$\bigotimes_{l=1}^d (\mathbf{A}_l \mathbf{D}_l) = \left(\bigotimes_{l=1}^d \mathbf{A}_l \right) \left(\bigotimes_{l=1}^d \mathbf{D}_l \right) \quad (\text{B.8})$$

This can be generalised further. For example,

$$\bigotimes_{l=1}^d (\mathbf{A}_l \mathbf{D}_l \mathbf{B}_l) = \left(\bigotimes_{l=1}^d \mathbf{A}_l \right) \left(\bigotimes_{l=1}^d \mathbf{D}_l \right) \left(\bigotimes_{l=1}^d \mathbf{B}_l \right) \quad (\text{B.9})$$

6. Matrix vector product

$$(\mathbf{A}_l \otimes \mathbf{B}_l) \mathbf{v} = \text{vec}(\mathbf{B}_l \mathbf{V} \mathbf{A}_l^\top) \quad (\text{B.10})$$

where $\mathbf{V} = \text{vec}^{-1}(\mathbf{v})$ is the inverse of the vectorization operator and \mathbf{v} is a vector of length $m_l q_l$.

B.2 Eigen-decomposition of a Gram matrix with Kronecker product

Assume a tensor product kernel

$$k(\mathbf{x}, \mathbf{x}') = \prod_{l=1}^d k_d(\mathbf{x}_l, \mathbf{x}'_l)$$

over a multidimensional grid $\mathcal{D} = \mathcal{D}_1 \times \dots \times \mathcal{D}_d$ where $\mathbf{x}_l \in \mathcal{D}_l$ and each k_l is defined on \mathcal{D}_l . Let n_l denote the dimension of each grid. Then the associated Gram matrix can be written as

$$\mathbf{K} = \bigotimes_{l=1}^d \mathbf{K}_l \quad (\text{B.11})$$

where \mathbf{K}_l is a $n_l \times n_l$ gram matrix for l input dimension, with i, j -th element given by $k_l(\mathbf{x}_{(l),i}, \mathbf{x}_{(l),j})$. Let $\mathbf{K}_l = \mathbf{Q}_l \mathbf{\Lambda}_l \mathbf{Q}_l^\top$ be eigen-decomposition of each matrix. Then the eigen-decomposition of the matrix \mathbf{K} is the following:

$$\begin{aligned} \mathbf{K} &= \bigotimes_{l=1}^d (\mathbf{Q}_l \mathbf{\Lambda}_l \mathbf{Q}_l^\top) \\ &= \bigotimes_{l=1}^d \mathbf{Q}_l \bigotimes_{l=1}^d \mathbf{\Lambda}_l \bigotimes_{l=1}^d \mathbf{Q}_l^\top. \end{aligned} \quad (\text{B.12})$$

Note that $\mathbf{Q} \equiv \bigotimes_{l=1}^d \mathbf{Q}_l$ is orthonormal, i.e., $\mathbf{Q}\mathbf{Q}^\top = \mathbf{I}_n$. We can confirm this by

$$\begin{aligned} \mathbf{Q}\mathbf{Q}^\top &= \left(\bigotimes_{l=1}^d \mathbf{Q}_l \right) \left(\bigotimes_{l=1}^d \mathbf{Q}_l \right)^\top = \left(\bigotimes_{l=1}^d \mathbf{Q}_l \right) \left(\bigotimes_{l=1}^d \mathbf{Q}_l^\top \right) \\ &= \bigotimes_{l=1}^d \mathbf{Q}_l \mathbf{Q}_l^\top = \bigotimes_{l=1}^d \mathbf{I}_{n_l} = \mathbf{I}_n. \end{aligned} \quad (\text{B.13})$$

An example with fractional Brownian motion kernel

This decomposition leads to a particularly efficient algorithm when using fBM kernel or squared fBM kernel with a known Hurst coefficient γ_l . Let each k_l be a fBM $_{\gamma_l}$ kernel. This means that we have only one hyper-parameter (scale parameter) to estimate for each dimension l . We denote the corresponding gram matrix by $\mathbf{K}_l = \alpha_l \mathbf{K}'_l$ where \mathbf{K}'_l is un-scaled gram matrix. Let $\mathbf{K}'_l = \mathbf{Q}_l \mathbf{\Lambda}_l \mathbf{Q}_l^\top$ be the eigen-decomposition of the un-scaled matrix. Then eigen-decomposition of \mathbf{K}_l is

$$\mathbf{K}_l = \alpha_l \mathbf{K}'_l = \mathbf{Q}_l (\alpha_l \mathbf{\Lambda}_l) \mathbf{Q}_l^\top.$$

Using (B.12), we can write

$$\mathbf{K} = \bigotimes_{l=1}^d \mathbf{K}'_l = \bigotimes_{l=1}^d \mathbf{Q}_l \bigotimes_{l=1}^d (\alpha_l \mathbf{\Lambda}_l) \bigotimes_{l=1}^d \mathbf{Q}_l^\top. \quad (\text{B.14})$$

This suggests that when estimating the hyperparameters by maximising the marginal likelihood or by MCMC, we do not have to apply eigen-decomposition at each iteration. By simply multiplying each eigenvalue by the scale parameters, the inverse and the determinant can be updated.

C Application

C.1 Data manipulation

Missing value imputation

In the dataset used in this paper, we had 1290 missing value out of 208152. For each missing value at a measurement site, we created a small subset of the data consisting of the observations collected from the same site from 24 hours before to 24 hours after the missing values is observed. A simple one dimensional Gaussian process regression with squared and centred standard ($\gamma = \frac{1}{2}$) Brownian Motion kernel is then fitted. We replace the missing value with the posterior predictive mean given in (2.20).

Adjustment of Summer time

The study period, which spans from the 6th of January 2020 to the 31st of May, 2020, includes the clock change to British Summer Time (BST), started on 1:00 AM on March 29. The timestamp in the original data are all in Greenwich Mean Time (GMT). We converted the timestamp to match BST from 1:00 AM (in GMT) forward. This resulted in one hour gap without any record at 1:00 AM of the adjusted timestamp. We filled the gap with a mean of the record before and after. The procedure is summarised in the table below.

Original time in GMT	Original y	Time in BST	Adjusted time	y after adjustment
\vdots	\vdots	\vdots	\vdots	\vdots
2020-03-29 0:00AM	y_{t-1}	-	2020-03-29 0:00AM	y_{t-1}
2020-03-29 1:00AM	y_t	2020-03-29 2:00AM	2020-03-29 1:00AM	$(y_{t-1} + y_t)/2$
2020-03-29 2:00AM	y_{t+1}	2020-03-29 3:00AM	2020-03-29 2:00AM	y_t
2020-03-29 3:00AM	y_{t+1}	2020-03-29 3:00AM	2020-03-29 3:00AM	y_{t+1}
\vdots	\vdots	\vdots	\vdots	\vdots

C.2 Gram matrix for each models

Let \mathbf{K}_l denote the Gram matrix that corresponds with the kernel k_l in Section 4.2, i.e., $\mathbf{K}_l = \{k_{i,j}^{(l)}\}_{1 \leq i,j \leq n_l}$. The Gram matrix for the models under consideration in Section 4.2 are listed as follows.

- Model 1: main effect

$$\mathbf{K}_{m1} = \bigotimes_{l=1}^3 \mathbf{1}\mathbf{1}_{n_l}^\top + \mathbf{K}_1 \otimes \mathbf{1}\mathbf{1}_{n_2}^\top \otimes \mathbf{1}\mathbf{1}_{n_3}^\top + \mathbf{1}\mathbf{1}_{n_1}^\top \otimes \mathbf{K}_2 \otimes \mathbf{1}\mathbf{1}_{n_3}^\top + \mathbf{1}\mathbf{1}_{n_1}^\top \otimes \mathbf{1}\mathbf{1}_{n_2}^\top \otimes \mathbf{K}_3$$

- Model 2: space-time interactions

$$\mathbf{K}_{m2} = \mathbf{K}_{m1} + \mathbf{K}_1 \otimes \mathbf{K}_2 \otimes \mathbf{1}\mathbf{1}_{n_3}^\top + \mathbf{K}_1 \otimes \mathbf{1}\mathbf{1}_{n_2}^\top \otimes \mathbf{K}_3$$

- Model 3: all two-way interactions

$$\mathbf{K}_{m3} = \mathbf{K}_{m2} + \mathbf{1}\mathbf{1}_{n_1}^\top \otimes \mathbf{K}_2 \otimes \mathbf{K}_3$$

- Model 4: saturated

$$\mathbf{K}_{m4} = \mathbf{K}_{m3} + \mathbf{K}_1 \otimes \mathbf{K}_2 \otimes \mathbf{K}_3$$

- Model 5: three-way interaction only

$$\mathbf{K}_{m5} = \mathbf{K}_1 \otimes \mathbf{K}_2 \otimes \mathbf{K}_3$$

References

- Adler, R. J. (1981). *The geometry of random fields*. John Wiley & Sons.
- Aronszajn, N. (1950). Theory of reproducing kernels. *Transactions of the American mathematical society*, 68(3), 337–404.
- Bergsma, W. P. (2020). Regression with i-priors. *Econometrics and Statistics*, 14, 89–111.
- Cameletti, M. (2020). The effect of corona virus lockdown on air pollution: Evidence from the city of brescia in lombardia region (italy). *Atmospheric Environment*, 239, 117794.
- Cooper, M. J., Martin, R. V., Hammer, M. S., Levelt, P. F., Veefkind, P., Lamsal, L. N., Krotkov, N. A., Brook, J. R., & McLinden, C. A. (2022). Global fine-scale changes in ambient no2 during covid-19 lockdowns. *Nature*, 601(7893), 380–387.
- Datta, A., Banerjee, S., Finley, A. O., Hamm, N. A., & Schaap, M. (2016). Nonseparable dynamic nearest neighbor gaussian process models for large spatio-temporal data with an application to particulate matter analysis. *The annals of applied statistics*, 10(3), 1286.
- Diggle, P. J., Moraga, P., Rowlingson, B., & Taylor, B. M. (2013). Spatial and spatio-temporal log-Gaussian Cox processes: extending the geostatistical paradigm. *Statistical Science*, 542–563.
- Durrande, N., Ginsbourger, D., Roustant, O., & Carraro, L. (2013). Anova kernels and rkhs of zero mean functions for model-based sensitivity analysis. *Journal of Multivariate Analysis*, 115, 57–67.
- Dutta, V., Kumar, S., & Dubey, D. (2021). Recent advances in satellite mapping of global air quality: Evidences during covid-19 pandemic. *Environmental Sustainability*, 1–19.
- Duvenaud, D., Nickisch, H., & Rasmussen, C. (2011). Additive gaussian processes. *Advances in Neural Information Processing Systems*, 24.
- Embrechts, P., & Maejima, M. (2002). Selfsimilar processes, princeton ser. *Appl. Math., Princeton University Press, Princeton, NJ*.
- Fioravanti, G., Cameletti, M., Martino, S., Cattani, G., & Pisoni, E. (2022). A spatiotemporal analysis of no 2 concentrations during the italian 2020 covid-19 lockdown. *Environmetrics*, 33(4), e2723.
- Flaxman, S., Wilson, A., Neill, D., Nickisch, H., & Smola, A. (2015). Fast kronecker inference in gaussian processes with non-gaussian likelihoods. In F. Bach & D. Blei (Eds.). PMLR. <http://proceedings.mlr.press/v37/flaxman15.html>
- Genton, M. G. (2001). Classes of kernels for machine learning: A statistics perspective. *Journal of machine learning research*, 2(Dec), 299–312.
- Gilboa, E., Saatçi, Y., & Cunningham, J. P. (2013). Scaling multidimensional inference for structured gaussian processes. *IEEE transactions on pattern analysis and machine intelligence*, 37(2), 424–436.
- Grancharova, A., Kocijan, J., & Johansen, T. A. (2008). Explicit stochastic predictive control of combustion plants based on gaussian process models. *Automatica*, 44(6), 1621–1631.
- Groot, P., Peters, M., Heskes, T., & Ketter, W. (2014). Fast laplace approximation for gaussian processes with a tensor product kernel.
- Hastie, T., & Tibshirani, R. (1990). *Generalized additive models*. Wiley Online Library.
- Higham, J., Ramírez, C. A., Green, M., & Morse, A. (2021). Uk covid-19 lockdown: 100 days of air pollution reduction? *Air Quality, Atmosphere & Health*, 14, 325–332.
- Jamil, H. (2018). *Regression modelling using priors depending on fisher information covariance kernels (i-priors)* (Doctoral dissertation). London School of Economics and Political Science.
- Jamil, H., & Bergsma, W. (2020). Bayesian variable selection for linear models using i-priors. *Theoretical, modelling and numerical simulations toward industry 4.0* (pp. 107–132). Springer.

- Jephcote, C., Hansell, A. L., Adams, K., & Gulliver, J. (2021). Changes in air quality during COVID-19 ‘lockdown’ in the United Kingdom. *Environmental Pollution*, 272, 116011.
- Krige, D. G. (1951). A statistical approach to some basic mine valuation problems on the witwatersrand. *Journal of the Chemical, Metallurgical and Mining Society of South Africa*, 52, 119–139.
- Lee, D. (2011). A comparison of conditional autoregressive models used in bayesian disease mapping. *Spatial and spatio-temporal epidemiology*, 2(2), 79–89.
- Lee, J. D., Drysdale, W. S., Finch, D. P., Wilde, S. E., & Palmer, P. I. (2020). UK surface NO₂ levels dropped by 42% during the covid-19 lockdown: Impact on surface O₃. *Atmospheric Chemistry and Physics*, 20(24), 15743–15759.
- Liu, H., Ong, Y.-S., Shen, X., & Cai, J. (2020). When Gaussian process meets big data: A review of scalable GPs. *IEEE transactions on neural networks and learning systems*, 31(11), 4405–4423.
- Liu, H., Yang, C., Huang, M., Wang, D., & Yoo, C. (2018). Modeling of subway indoor air quality using gaussian process regression. *Journal of hazardous materials*, 359, 266–273.
- MacKay, D. J. (1995). Probable networks and plausible predictions—a review of practical bayesian methods for supervised neural networks. *Network: computation in neural systems*, 6(3), 469.
- Matérn, B. (1960). *Spatial variation*. Allmänna Förlaget.
- Matheron, G. (1963). Principles of geostatistics. *Economic Geology*, 58, 1246–1266.
- Møller, J., Syversveen, A. R., & Waagepetersen, R. P. (1998). Log Gaussian Cox processes. *Scandinavian journal of statistics*, 25(3), 451–482.
- Murray, I., & Ghahramani, Z. (2005). A note on the evidence and bayesian occam’s razor. *Gatsby Computational Neuroscience Unit Tech Report*, 1–4.
- Patel, Z. B., Purohit, P., Patel, H. M., Sahni, S., & Batra, N. (2022). Accurate and scalable gaussian processes for fine-grained air quality inference. *Proceedings of the AAAI Conference on Artificial Intelligence*, 36(11), 12080–12088.
- Petelin, D., Grancharova, A., & Kocijan, J. (2013). Evolving gaussian process models for prediction of ozone concentration in the air. *Simulation modelling practice and theory*, 33, 68–80.
- Pinder, T., Hollaway, M., Nemeth, C., Young, P. J., & Leslie, D. (2021). A probabilistic assessment of the covid-19 lockdown on air quality in the uk. *arXiv preprint arXiv:2104.10979*.
- Plate, T. A. (1999). Accuracy versus interpretability in flexible modeling: Implementing a tradeoff using gaussian process models. *Behaviormetrika*, 26(1), 29–50.
- Rasmussen, C. E., & Williams, C. K. (2006). *Gaussian processes for machine learning* (Vol. 1). MIT press.
- Saatçi, Y. (2012). *Scalable inference for structured gaussian process models* (Doctoral dissertation). University of Cambridge.
- Solberg, S., Walker, S.-E., Schneider, P., & Guerreiro, C. (2021). Quantifying the impact of the covid-19 lockdown measures on nitrogen dioxide levels throughout europe. *Atmosphere*, 12(2), 131.
- Stein, M. L. (1999). *Interpolation of spatial data: Some theory for kriging*. Springer Science & Business Media.
- Stitson, M., Gammerman, A., Vapnik, V., Vovk, V., Watkins, C., & Weston, J. (1999). Support vector regression with anova decomposition kernels. advanced in kernel methods: Support vector learning.
- Titsias, M. (2009). Variational learning of inducing variables in sparse gaussian processes. *Artificial intelligence and statistics*, 567–574.

- Wahba, G., Wang, Y., Gu, C., Klein, R., & Klein, B. (1995). Smoothing spline anova for exponential families, with application to the wisconsin epidemiological study of diabetic retinopathy: The 1994 neyman memorial lecture. *The Annals of Statistics*, 23(6), 1865–1895.
- Williams, C., & Seeger, M. (2001). Using the Nyström method to speed up kernel machines. *Advances in neural information processing systems*, 13.
- Wilson, A. G., Gilboa, E., Nehorai, A., & Cunningham, J. P. (2014). Fast kernel learning for multidimensional pattern extrapolation. *Advances in neural information processing systems*, 27.